Corresponding author: M. T. Rodgers, email: mrodgers@chem.wayne.edu, Tel. (313)577-2431

Structural Determination of Lysine-Linked Cisplatin Complexes via IRMPD Action Spectroscopy: NN_s and NO^- Binding Modes of Lysine to Platinum Coexist

C. C. He,[a] L. A. Hamlow,[a] H. A. Roy,[a] Zachary. J. Devereaux,[a] M. A. Hasan, [a] E. Israel,[a] N. A. Cunningham,[a] J. Martens,[b] G. Berden,[b] J. Oomens,[b,c] and M. T. Rodgers[a,*]

[a]*Department of Chemistry, Wayne State University, Detroit, Michigan 48202, United States*
[b]*Radboud University, Institute for Molecules and Materials, FELIX Laboratory, Toernooiveld 7, 6525ED Nijmegen, The Netherlands*
[c]*van't Hoff Institute for Molecular Sciences, University of Amsterdam, Science Park 904, 1098xH, Amsterdam,The Netherlands*

ABSTRACT

Despite its success as an anticancer drug, cisplatin suffers from resistance and produces side effects. To overcome these limitations, amino acid-linked cisplatin analogues have been investigated. Lysine-linked cisplatin, Lysplatin, (Lys)$PtCl_2$, exhibited outstanding reactivity towards DNA and RNA that differs from that of cisplatin. To gain insight into its differing reactivity, the structure of Lysplatin is examined here using infrared multiple photon dissociation (IRMPD) action spectroscopy. To probe the influence of the local chemical environment on structure, the deprotonated and sodium cationized Lysplatin complexes are examined. Electronic structure calculations are performed to explore possible modes of binding of Lys to Pt, their relative stabilities, and to predict their infrared spectra. Comparisons of the measured IRMPD and predicted IR spectra elucidate the structures contributing to the experimental spectra. Coexistence of two modes of binding of Lys to Pt are found where Lys binds via the backbone and side chain amino nitrogen atoms, NN_s, or to the backbone amino and carboxylate oxygen atoms, NO^-. Glycine-linked cisplatin and arginine-linked cisplatin complexes have previously been found to bind only via the NO^- binding mode. Present results suggest that the NN_s binding conformers may be key to the outstanding reactivity of Lysplatin toward DNA and RNA.

INTRODUCTION

Cisplatin (cis-diamminedichloroplatinum, Figure 1) is a well-known anticancer drug that has been in use for more than fifty years.[1-3] Although cisplatin was first discovered in 1845, it wasn't until Rosenberg's identification of cisplatin and its biologic actions in 1965 that its therapeutic application was recognized. Since 1978 cisplatin has been applied in a variety of cancer treatments, including testicular, ovarian, head, neck, bladder, and lung cancers.[4-6] Previous studies suggest that cisplatin binds to DNA and RNA strands via coordination to the N7 position of purine bases, with a preference for guanine (G) over adenine (A) residues.[1,2,7,8] Cisplatin also suffers drawbacks, including severe side effects (e.g., neurotoxicity and nephrotoxicity), resistance, and low cell accumulation.[9-12]

It is believed that the chlorido ligands of cisplatin are labile and prominently determine the rate of adduct formation; the ammonia molecules are carrier ligands predominantly determining the coordination sites of cisplatin to DNA or RNA strands[10,13,14] and to amino acids.[15-17] In an attempt to alter the reactivity and ideally improve the performance of cisplatin, amino acids are examined as replacements for the ammonia ligands in cisplatin. All amino acids provide backbone amino and carboxylic acid functionalities that may potentially bind to the Pt metal center. The diverse side chains found among canonical and noncanonical amino acids also expand the pool of potential binding sites to the Pt metal center in amino acid-linked cisplatin analogues.[18] In an investigation of 17 amino acid-linked platinum complexes, lysine-linked cisplatin, Lysplatin, (Lys)$PtCl_2$, (see Figure 1) exhibited moderate cytotoxicity and reactivity at all d(AG) and d(GG) sequences along DNA strands in vitro; reactivity that differs from cisplatin which reacts at d(GG) sequences.[19] Lysplatin also exhibited a binding preference for r(AG) and r(GA) sequences of ribosomal RNA (rRNA), whereas cisplatin prefers binding to r(GG) sequences.[20] The altered reactivity of Lysplatin suggests that it may be useful as a potential anticancer drug or an alternative and complementary chemical probe after cisplatin.[21]

Similar to other amino acid-linked platinum complexes, the mode of binding of Lys to the Pt center in Lysplatin has been interpreted as an NO^- binding structure in the neutral state as

determined by x-ray crystallography measurements.[19,20,22-25] In the study of diaminocarboxylate [Dac, $HO_2C(NH_2)CH(CH_2)_nNH_2$] linked platinum complexes, 2,3-diaminopropionate (Dap, n=1), 2,4-diaminobutyrate (Dab, n=2), ornithine (Orn, n=3), and Lys (n=4) were examined.[26-28] Dap and Dab were found to bind to Pt via NN_s or NO^- modes depending on reaction conditions. In contrast, both Orn and Lys were interpreted as binding to Pt via the NO^- mode as a C=O stretch was not observed in the IR fingerprint region.[27] In a later study of $(Dap)PtCl_2$ and $(Dab)PtCl_2$ and their ethyl ester derivatives $(Dap\text{-}H+Et)PtCl_2$ and $(Dab\text{-}H+Et)PtCl_2$, higher antitumor activity was observed for their ethyl ester derivatives.[29] The authors hypothesized that the ethyl ester derivatives of Dap and Dab bind to Pt via the NN_s binding mode under the experimental conditions employed in that work. The increased antitumor activity of the ethyl ester derivatives was explained by their neutral ester group more readily penetrating the nonpolar cell membrane, whereas the negatively charged carboxylate groups of the $[(Dap\text{-}H)PtCl_2]^-$ and $[(Dab\text{-}H)PtCl_2]^-$ complexes may hinder their penetration of the cell membrane.[18,29,30] A study with HeLa cells indicated that Lysplatin suffers from low cellular uptake, which again may be related to inefficient cell penetration.[30] If only NO^- binding complexes of Lysplatin are formed, the overall positive charge of the complex would be expected to facilitate cell penetration leaving the low uptake of Lysplatin unexplained.[19] However, if Lys binds to Pt via the NN_s binding mode, the low cellular uptake would be easily understood. Previous gas-phase studies of the amino acid-linked platinum complexes of glycine (Gly) and arginine (Arg) determined that Gly and Arg bind to Pt only via the backbone nitrogen and carboxylate oxygen atoms, i.e. the NO^- binding mode.[24,25] However, if Lys binds to the Pt metal center only via the NO^- binding mode, the reactivity of Lysplatin should be similar to that of Glyplatin and Argplatin, and the outstanding reactivity of Lysplatin observed in the screening of amino acid-linked platinum complexes would not be easily explained.[19]

In the present study, infrared multiple photon dissociation (IRMPD) action spectroscopy experiments complemented by computational predictions are used to reinvestigate the structure of Lysplatin in its deprotonated and sodium cationized forms, $[(Lys\text{-}H)PtCl_2]^-$ and $[(Lys)PtCl_2+Na]^+$, to mimic different chemical environments. To best compare to the solid-phase IR spectrum, which

does not exhibit a strong C=O stretch, deprotonated Lysplatin was first investigated to evaluate the spectral similarities between the condensed and gas-phase structures when the carboxylic acid moiety is deprotonated.[27] Sodium cationization enables Lysplatin to adopt an overall neutral charge state in the complex. In previous structural studies of protonated and alkali metal cationized Lys, charge-solvated structures (i.e., nonzwitterionic) were populated as evidenced by observation of a strong C=O stretch above 1700 cm^{-1} in all cases.[31-34] A strong C=O stretch should also be observed for the $[(Lys)PtCl_2+Na]^+$ complex if Lys adopts a similar nonzwitterionic structure. The structural and energetic information garnered from calculations for the $[(Lys\text{-}H)PtCl_2]^-$ and $[(Lys)PtCl_2+Na]^+$ complexes enable comprehensive investigation of all possible binding modes of Lys to the Pt center and their relative stabilities. Comparisons among these two systems further elucidate the influence of the local environment on the mode of binding. Comparisons of predicted IR spectra with experimentally measured IRMPD spectra enable determination of the structures of these Lysplatin complexes that are populated in the experiments. Present results are also compared to those based on the x-ray crystal structure of Lysplatin previously reported.[19,20,22-25]

EXPERIMENTAL AND COMPUTATIONAL METHODS

IRMPD Action Spectroscopy. Lysplatin was synthesized and purified using procedures reported previously.[19,20,22,35,36] IRMPD action spectra of the $[(Lys\text{-}H)PtCl_2]^-$ and $[(Lys)PtCl_2+Na]^+$ complexes in the IR fingerprint region were obtained using a modified 3D quadrupole ion trap mass spectrometer (Bruker, amaZon Speed ETD, Billerica, MA) coupled with the tunable free electron laser (FEL) at the FELIX Laboratory (Nijmegen, the Netherlands). Details of the instrumental setup have been reported previously.[37-40] The IRMPD action spectrum of the $[(Lys)PtCl_2+Na]^+$ complex in the hydrogen-stretching region was obtained using a similar ion trap mass spectrometer (Bruker, amaZon ETD, Billerica, MA) coupled to a YAG-pumped tunable IR OPO/OPA laser system (optical parametric oscillator/amplifier, LaserVision, Bellevue, WA) in our laboratory at Wayne State University (WSU). The experimental setup has been described in detail elsewhere.[41] Due to the very low absorbance of the vibrational modes in the hydrogen-

stretching region, the IRMPD action spectrum of the $[(Lys\text{-}H)PtCl_2]^-$ complex was acquired using a Fourier transform ion cyclotron resonance mass spectrometer (FT-ICR MS, Bruker, solariX, Billerica, MA) coupled to the same OPO/OPA laser in our laboratory at WSU. Lysplatin was dissolved in a 50:50 (v/v) methanol:water mixture and diluted to a concentration of 5–10 μM for use in the experiments examining the $[(Lys\text{-}H)PtCl_2]^-$ complex. A solution containing 10 μM of Lysplatin and NaCl in a 50:50 (v/v) methanol:water mixture was used to generate the $[(Lys)PtCl_2+Na]^+$ complex ions. In all experiments, the ions were generated by electrospray ionization (ESI), guided by rf ion funnels and rf ion guides, mass isolated in the quadrupole ion trap or ICR cell, and then irradiated by the FEL or OPO/OPA laser. The FELIX FEL provides pulse energies of 20–60 mJ per 5–10 μs macropulse at a 10 Hz repetition rate and with a 0.4% bandwidth. The OPO/OPA provides pulse energies of 15-20 mJ (6 ns, 10 Hz) with a bandwidth of 3 cm^{-1}. When the laser frequency is resonant with a vibrational mode of the precursor Lysplatin complex, the ion absorbs a photon and undergoes rapid redistribution of the photon energy into the bath of internal modes available, resulting in relaxation of the excited vibrational mode to its ground state. The photon absorption process repeats tens to hundreds of times and eventually leads to fragmentation of the precursor ion when its internal energy exceeds the threshold of dissociation. For experiments in the IR fingerprint region, two macropulses were applied in each scan to ensure sufficient photon absorption. The IRMPD spectrum of the $[(Lys\text{-}H)PtCl_2]^-$ complex acquired is based on the average of six mass scans over the frequency range of ~600–1900 cm^{-1} with 3–8 dB attenuation. The IRMPD spectra of the $[(Lys)PtCl_2+Na]^+$ complex acquired is the result of the average of eight mass scans in the frequency range of ~600–1900 cm^{-1} with 0–3 dB attenuation. The IR laser frequency was calibrated using a grating spectrometer. The IRMPD spectra measured for the $[(Lys\text{-}H)PtCl_2]^-$ and $[(Lys)PtCl_2+Na]^+$ complexes in the IR hydrogen-stretching region are based on the average of three to four mass scans with an irradiation time of 2 and 20 s, respectively, and were acquired over the range of ~2800–3650 cm^{-1}. The IRMPD yield was calculated as the ratio of the sum of the intensities of all fragment ions versus the total ion intensity as shown in eq 1,

$$\text{IRMPD yield} = \sum I_{f_i} / (I_p + \sum I_{f_i}) \quad (1)$$

where I_{f_i} and I_p are the measured ion intensities of the fragment and precursor ions, respectively. The IRMPD yield was linearly corrected for the frequency-dependent variations in the laser power.[42]

Computational Details. Candidate structures of the $[(\text{Lys-H})\text{PtCl}_2]^-$ and $[(\text{Lys})\text{PtCl}_2+\text{Na}]^+$ complexes were constructed that included all plausible bidentate interactions between Lys and Pt with the chlorido ligands coordinated to the Pt center in a *cis* fashion.[19,26-28] Various favorable modes of sodium cation binding were also examined for each binding mode of Lys to the Pt metal center. The structural sampling process employed here is similar to that reported in our previous investigation of the analogous Argplatin complexes.[25] Briefly, candidate structures for the $[(\text{Lys-H})\text{PtCl}_2]^-$ and $[(\text{Lys})\text{PtCl}_2+\text{Na}]^+$ complexes were optimized using Gaussian 09 and the B3LYP/mDZP/def2-TZVP hybrid approach, where B3LYP is the density functional method, mDZP is the basis set used for Pt, and def2-TZVP the basis set employed for all other atoms.[24,25,43] All basis sets were acquired from the EMSL basis set exchange library.[45,46] Optimized structures and partial charges were extracted for molecular mechanics (MM) calculations using HyperChem software, to relax the side chain of Lys and explore the conformational space available to that structure.[47,48] The MM+ force field was used for the simulated annealing process.[49,50] Parameters for Pt have been developed and validated to work with the MM+ force field.[51,52] The simulated annealing procedures employed here have been described in our previous IRMPD studies.[25,53-59] Energy restrictions were imposed on angles and dihedral angles involving the Pt center in order to maintain a roughly square planar shape of the Pt coordination sphere.[25] Approximately 30 of the 300 candidate structures generated via simulated annealing for each mode of binding were selected based on their relative Gibbs energies calculated at the molecular mechanics level and submitted for further optimization at the B3LYP/mDZP/def2-TZVP level of theory. Relative Gibbs energies at 298 K were extracted, and the linear IR spectra predicted for these structures were compared with the IRMPD spectra. Based on previous results for the deprotonated Glyplatin complex,

$[(Gly\text{-}H)PtCl_2]^-$, the computed frequencies were scaled by a factor of 0.970 and convoluted over a Gaussian line shape having a full width at half max (fwhm) of 20 cm^{-1} in the IR fingerprint region. To better fit the experimental spectra in the hydrogen-stretching region, computed frequencies were scaled by 0.957 for the $[(Lys\text{-}H)PtCl_2]^-$ complex and 0.960 for the $[(Lys)PtCl_2+Na]^+$ complex, and convoluted with a 10 cm^{-1} fwhm Gaussian lineshape to generate the theoretical IR spectra.[24,25] Implicit solvation calculations were also performed for representative low-energy conformers to help rationalize differences observed in the experiments vs. theoretical predictions. The default polarizable continuum model (PCM) using the integral equation formalism variant (IEFPCM) in the Gaussian 09 suite of programs was applied in those calculations, with the solvent set as water.[44] Relative Gibbs energies of implicit water-solvated conformers were also calculated at B3LYP/mDZP/def2-TZVP level of theory.

RESULTS

IRMPD Action Spectroscopy. The fragmentation behavior of Lysplatin in the gas phase may provide insight into its outstanding reactivity. Multiple photodissociation pathways were observed for both the $[(Lys\text{-}H)PtCl_2]^-$ and $[(Lys)PtCl_2+Na]^+$ complexes. Discussion of the observed fragmentation pathways is deferred to the discussion section following determination of the structure(s) of Lysplatin populated in the experiments.

The IRMPD spectra of the $[(Lys\text{-}H)PtCl_2]^-$ and $[(Lys)PtCl_2+Na]^+$ complexes are compared with the IRMPD spectra of the $[(Gly\text{-}H)PtCl_2]^-$, $[(Arg\text{-}H)PtCl_2]^-$, and $[(Arg)PtCl_2+Na]^+$ complexes previously investigated[24,25] in Figure 2. The Argplatin spectra were scaled down by a factor of four to facilitate the comparisons. The experimental IRMPD spectra of all three deprotonated amino acid-linked platinum complexes are highly parallel. However, the side chain of Lys produces several differences in the spectrum that facilitate differentiation of the $[(Gly\text{-}H)PtCl_2]^-$ and $[(Lys\text{-}H)PtCl_2]^-$ complexes including broadening of the feature at ~1300 cm^{-1} (which is associated C–H wagging and twisting of the backbone and side chain), a blue shift in the feature at ~1050 cm^{-1} (arising from NH_2 wagging), and disappearance of the feature at ~3300 cm^{-1} (associated with

symmetric NH_2 stretching and suggesting that hydrogen-bonding interactions may have eliminated the NH_2 symmetric stretch). The $[(Arg\text{-}H)PtCl_2]^-$ complex is more readily differentiated from the $[(Lys\text{-}H)PtCl_2]^-$ and $[(Gly\text{-}H)PtCl_2]^-$complexes as several additional spectral features and much more extensive broadening of the feature near 1300 cm^{-1} as well as broadening to the red of the feature near 1670 cm^{-1} arise from the guanidino moiety of the side chain of Arg. The IRMPD yields for $[(Gly\text{-}H)PtCl_2]^-$ and $[(Lys\text{-}H)PtCl_2]^-$ are also significantly lower than that of $[(Arg\text{-}H)PtCl_2]^-$; as such, the reduced laser power available in the hydrogen-stretching region may result in the dissociation thresholds not being reached for weak absorptions such that those features may be unobserved.

The IRMPD spectra of the $[(Lys)PtCl_2+Na]^+$ and $[(Arg)PtCl_2+Na]^+$ complexes exhibit obvious differences in both the IR fingerprint and hydrogen-stretching regions. An IR band at ~1750 cm^{-1} is observed in the spectrum of $[(Lys)PtCl_2+Na]^+$, indicating the presence of a free carbonyl stretch. It has been determined previously that $[(Arg)PtCl_2+Na]^+$ adopts the NO^- binding mode of Arg to the Pt metal center.[25] Hence, in $[(Arg)PtCl_2+Na]^+$, the bond order of the carbonyl moiety is closer to 1.5 than 2. The dominant IR band of $[(Lys)PtCl_2+Na]^+$ at ~1600 cm^{-1} is red shifted compared to that of $[(Arg)PtCl_2+Na]^+$, which is probably related to different hydrogen-bonding interactions involving the carboxylic acid/carboxylate moiety. $[(Lys)PtCl_2+Na]^+$ also exhibits fewer IR bands than $[(Arg)PtCl_2+Na]^+$ in the hydrogen-stretching region, which is of course related to the differences in the amino vs. guanidino side chain moieties of Lys vs. Arg.

Nomenclature. The nomenclature employed here to differentiate the various stable structures found for the deprotonated and sodium cationized Lysplatin complexes parallels that previously employed for the Argplatin analogues.[25] The modes of binding of Lys to Pt in the $[(Lys\text{-}H)PtCl_2]^-$ and $[(Lys)PtCl_2+Na]^+$ complexes are classified by their Pt chelating mode. When the binding mode to Pt involves a deprotonated or protonated site, it is indicated with a negative or positive sign, respectively. The backbone nitrogen is simply denoted as N, whereas the side chain nitrogen atom is designated as N_s, see Figure 1. The flexibility of the Lys side chain enables the formation of multiple stable conformers for each Pt chelating mode. The stable conformers

found for each Pt chelating mode are further designated with an underscore and a letter. The ground conformer is designated with an A, whereas excited conformers are designated with a letter (or letters) that are alphabetically incremented based on their relative Gibbs energies at 298 K, i.e., A, B, C, etc. In virtually all of the stable conformers determined for the $[(Lys)PtCl_2+Na]^+$ complex, the sodium cation binds between the two chlorido ligands. For these stable conformers no specific designation of the sodium cation binding mode is given. For the handful of high-energy conformers where the sodium cation binding mode differs, the Pt chelating mode is followed by an underscore and then the sodium chelating mode is given. When the sodium cation binding mode involves one or more of the chlorido ligands, they are denoted with a subscript that indicates the atom that it is *trans* to (e.g., Cl_b , Cl_O, and Cl_s denote Cl being *trans* to the backbone nitrogen, the carboxyl/carboxylate oxygen, and side chain nitrogen atoms, respectively). The two most favorable binding modes of the $[(Lys\text{-}H)PtCl_2]^-$ and $[(Lys)PtCl_2+Na]^+$ complexes, NN_s and NO^-, are shown schematically in Figure 1, whereas all low-energy conformers for all binding modes are compared in Figures S1 and S2, along with the naming designations.

Stable Structures and Relative Stabilities of Deprotonated Lysplatin. The stable low-energy structures found for the $[(Lys\text{-}H)PtCl_2]^-$ complex and their relative Gibbs energies calculated at B3LYP/mDZP/def2-TZVP level of theory are compared in Figure S1. All stable structures found with NN_s, NO^-, and N_sO^- binding modes are shown. Only the most stable conformer of the OO^- binding mode is shown due to its high relative Gibbs energy and misalignment of features found upon spectral comparison, consistent with findings for the $[(Gly\text{-}H)PtCl_2]^-$ and $[(Arg\text{-}H)PtCl_2]^-$ complexes.[24,25] Representative stable structures exhibiting different Pt chelating modes or different hydrogen-bonding interactions were selected and their relative Gibbs energies were further calculated using a polarizable continuum model (PCM) corresponding to water at the B3LYP/mDZP/def2-TZVP level of theory. The results are summarized in Table 1. Most maintained their structures upon solvation; however, several conformers, i.e., **NO^-_E**, **NO^-_I**, and **NO^-_AC**, lost one hydrogen-bonding interaction in the polarizable continuum as interactions with the solvent stabilize the free amino group. NN_s binding

structures exhibit low relative Gibbs energies in both the gas phase and in an aqueous polarizable continuum. The carboxylate group of NN_s binding structures generally forms a hydrogen bond with the backbone or side chain amino hydrogen atoms. A noncanonical hydrogen-bonding (dispersion) interaction between the carboxylate oxygen and backbone methylene hydrogen atoms may also stabilize the complex, e.g., see the **NN_s_C** and **NN_s_D** conformers of Figure S1. NN_s binding structures have less flexibility than the NO^- binding structures. The relative Gibbs energies of NO^- binding structures are at least 30 kJ/mol higher than NN_s structures in the gas phase, but the energy difference drops significantly, to ~10 kJ/mol or less in an aqueous polarizable continuum, indicating that NO^- binding structures are energetically competitive with NN_s binding structures in aqueous solution. Multiple types of hydrogen-bonding interactions are found among the computed NO^- binding structures. Those exhibiting interactions between the side chain amino group and the carboxylate group, **NO^-_E**, chlorido ligand, **NO^-_P**, backbone amino group and a chlorido ligand, **NO^-_Q**, and even with Pt, **NO^-_AC,** were found within 10 kJ/mol Gibbs energy of the most stable **NO^-_A** conformer. In NO^- binding structures, the neutral side chain amino group exhibits a weak preference for interacting with the $PtCl_2$ center rather than engaging in a hydrogen-bonding interaction with the deprotonated carboxylate moiety in the gas phase, compare conformers **NO^-_A** and **NO^-_B** vs. **NO^-_E** and **NO^-_G**, which all lie within 3 kJ/mol of one another. This trend is reversed in aqueous solution such that **NO^-_E** and **NO^-_G** are more stable by ~3 kJ/mol than **NO^-_A**. N_sO^- binding structures are less stable, by at least 40 kJ/mol in Gibbs energy than the ground **NN_s_A** conformer; this mode of binding also becomes relatively more stable in aqueous solution but are at least 25.0 kJ/mol less favorable than the ground **NN_s_A** conformer. N_sO^- binding structures exhibit various hydrogen-bonding interactions between the backbone amino group and the carboxylate moiety; for examples see the dual hydrogen-bonding interactions between the carboxylate oxygen atom and the backbone amino and methylene groups in the **N_sO^-_L** and **N_sO^-_N** conformers. Conformer **OO^-_A** exhibits a stretched side chain that is not stabilized by any hydrogen-bonding interactions. This structure is predicted to be much less stable in both the gas phase and aqueous polarizable continuum than the ground **NN_s_A** conformer,

97.6 vs. 92.0 kJ/mol; their high relative Gibbs energy likely due to the destabilization arising from the unfavorable ∠OPtO angle associated with this mode of binding.

Stable Structures and Relative Stabilities of Sodium Cationized Lysplatin. The stable low-energy conformers found for the $[(Lys)PtCl_2+Na]^+$ complex and their relative Gibbs energies at 298 K calculated at the B3LYP/mDZP/def2-TZVP level of theory are compared in Figure S2. Table 2 lists relative Gibbs energies of representative stable conformers in the gas phase and an aqueous polarizable continuum calculated at the B3LYP/mDZP/def2-TZVP level of theory. Only subtle differences were observed between the gas phase vs. aqueous polarizable continuum structures calculated. Similar to results for the $[(Lys\text{-}H)PtCl_2]^-$ complex, NN_s binding structures are predicted to be more stable than structures involving other modes of binding of Lys to the Pt center; the ground structure is again designated as **NN_s_A**. The NN_s binding structures are typically stabilized by hydrogen-bonding interactions between the carboxylic acid moiety and the backbone or side chain amino hydrogen atoms. The NO^- structures are less stable than NN_s structures by at least 32.6 kJ/mol in the gas phase but are of comparable stability to the NN_s structures in an aqueous polarizable continuum. All of the low-energy NO^- conformers are stabilized by a strong hydrogen-bonding (or salt bridge) interaction between the deprotonated carboxylate and protonated side chain amino moieties. Structures lacking this hydrogen-bonding interaction are ~70 kJ/mol less stable than the most stable **NO^-_A** conformer, and more than 100 kJ/mol higher in energy than the ground **NN_s_A** conformer. In particular, the side chain substituent of the **NO^-_X** conformer is fully extended in the typical anti staggered conformation that generally minimizes steric clashes; this conformer is predicted to be 140.3 kJ/mol less stable than the ground **NN_s_A** conformer in the gas phase, whereas in an aqueous environment it is quite stable and only 3.9 kJ/mol higher in Gibbs energy than the ground **NN_s_A** conformer. Stabilization of ionized functional groups is readily achieved in aqueous solution, whereas in the gas phase the formation of hydrogen-bonding and other noncovalent interactions provides stabilization where possible. Conformers **NO^-_A** and **NO_A** are the most stable zwitterionic and nonzwitterionic structures in which Lys binds to Pt via the backbone amino and carboxylic acid moieties; these conformers

differ by almost 30 kJ/mol in Gibbs energy (32.6 vs. 59.5 kJ/mol, respectively). In contrast, the **N_sO_A** nonzwitterionic and **N_sO^-_A** zwitterionic pair, only differ by ~4 kJ/mol in Gibbs energy (50.4 vs 54.5 kJ/mol), and in this case the nonzwitterionic conformer is more stable. The relative energy of the **NN_s_OCl_bCl_s_A** conformer falls between that of the NN_s and NO^- structures, which is not surprising given that the floppy side chain of Lys provides enough flexibility to enable interaction between the backbone oxygen and sodium cation. The **OO^-_A** conformer is again found to be very high in Gibbs energy both in the gas phase and in an aqueous polarizable continuum, 113.9 vs 94.8 kJ/mol; clearly this binding mode is unimportant. Conformers in which the sodium cation binds to the Lysplatin complex in an alternative fashion are also found (see other side chain binding modes of Figure S2), but these conformers are much less stable than the ground **NN_s_A** conformer. More interesting is that several conformers lose or change hydrogen-bonding interactions in the aqueous polarizable continuum, e.g., **NN_s_O**, **NO^-_F**, and **N_sO^-_J**, or the chelation mode of the sodium cation changes from bidentate to monodentate, **NN_s_OO_A** and **NO_N_sO_A**.

DISCUSSION

Interpretation of the IRMPD Spectrum of Deprotonated Lysplatin. The experimental IRMPD spectrum measured for the $[(Lys\text{-}H)PtCl_2]^-$ complex is compared to theoretical IR spectra predicted for several stable low-energy NN_s and NO^- binding conformers in Figure 3 that combined represent the experimental data very well. As can be seen in the figure, the NN_s and NO^- binding conformers exhibit relatively similar IR spectra in the IR fingerprint region; differences in the band positions of minor features establish the presence of both NN_s (1157 cm^{-1}) and NO^- (1046 cm^{-1}) conformers in the experiments. It is interesting to see that the predicted IR spectrum of the **NN_s_E** conformer provides a slightly better match to the IRMPD spectrum than the most stable gas-phase **NN_s_A** conformer, particularly considering the absence of the feature predicted at ~1520 cm^{-1}, but also in the alignment of the small feature observed at ~1580 cm^{-1} in the experimental data associated with NH_2 scissoring, and to a lesser extent in the alignment of the

dominant feature experimentally observed at ~1675 cm^{-1}. The better reproduction of the measured spectrum by the **NN_s_E** conformer is less surprising when it is appreciated that this conformer becomes the ground conformer in an aqueous polarizable continuum. Conformer **NN_s_C** exhibits reasonable agreement as well, but the feature associated with NH_2 scissoring is also shifted and appears at ~1550 cm^{-1} (see Figure S3). Further, this conformer is also predicted to be higher in Gibbs energy than the other two NN_s binding conformers. Thus, it is unlikely that the **NN_s_C** conformer is significantly populated in the experiments. The predicted spectra of the NO^- binding conformers in Figure 3 are highly parallel; all exhibit a free C=O stretch near 1675 cm^{-1}. When the carbonyl oxygen atom engages in a hydrogen-bonding interaction, the C=O stretch is influenced, and the predicted IR spectrum exhibits poorer alignment with the experimentally observed feature, see for examples conformers **NO^-_G** and **NO^-_L** of Figure S3. The other NO^- binding conformers shown in Figure S3 do not exhibit any unique IR bands that distinguish them from the low-energy NO^- binding structures compared in Figure 3. Thus, while their presence in the experiments cannot be ruled out based on the predicted vs. measured spectra, their higher predicted Gibbs energies suggest that they are not measurably populated in the experiments. Similar comparisons are made for select N_sO^- and OO^- binding conformers in Figure S4; extensive spectral misalignments indicate that these structures were not populated in the experiments.

The hydrogen-stretching region is not as helpful for structure/conformer differentiation as the relative intensities of the features predicted are very small (note the different relative intensity scale for the IR fingerprint vs. hydrogen-stretching regions) in the figures, and the laser output over this region is much weaker such that the threshold for dissociation may not be reached and many of these weak features are thus not experimentally observed. Both the low-energy NN_s and NO^- conformers compared in Figure 3 predict a feature than is well aligned with the single feature experimentally observed at ~3350 cm^{-1}. Combined the stable low-energy NN_s and NO^- binding conformers shown in Figure 3 best represent the experimental spectrum indicating that these conformers were likely accessed in the experiments. Detailed peak assignments for the spectral

features observed in the IRMPD spectrum and based primarily on the **NN_s_E** and **NO^-_A** conformers shown in Figure 3 are summarized in Table 3.

Interpretation of the IRMPD Spectrum of Sodium Cationized Lysplatin. The experimental IRMPD spectrum of the $[(Lys)PtCl_2+Na]^+$ complex is compared to the predicted IR spectra of select stable low-energy NN_s and NO^- binding conformers that combined reproduce the measured spectrum well in Figure 4. In the IR fingerprint region, the NN_s binding conformers uniquely contribute the band at ~1750 cm^{-1} (C=O stretch), whereas the NO^- binding conformers dominantly contribute the intense and broad unresolved features that appear at ~1600 cm^{-1}. Indeed, the lowest energy **NO^-_A** conformer provides the best match to the measured IRMPD spectrum for all features in the fingerprint region except the band at ~1750 cm^{-1}. The **NN_s_D** conformer is 4.1 kJ/mol less stable than the ground **NN_s_A** conformer in the gas phase, but is only 1.6 kJ/mol less stable in an aqueous polarizable continuum. The predicted spectrum of conformer **NN_s_D** reproduces the IR band at ~1750 cm^{-1} better than ground **NN_s_A** conformer, hence these two conformers are probably competing in solution. Small IR features at ~1700 and 1720 cm^{-1} (note that the peak splitting is real) are well represented by the computed IR spectra of the **NN_s_B** and **NO^-_X** conformers, suggesting their presence in low abundance in the experiments. The large relative Gibbs energy of the **NO^-_X** conformer in the gas phase, 140.3 kJ/mol, suggests that this structure is experimentally unimportant. However, the dangling protonated side chain of this conformer is greatly stabilized in an aqueous polarizable continuum with a Gibbs energy of 3.9 kJ/mol such that it is competitive with the most stable NN_s binding conformers. The **NO^-_H** conformer contributes the shoulder to the red of the most intense peak near ~1550 cm^{-1}, and it is also predicted to be the most stable NO^- binding conformer in an aqueous polarizable continuum, only 0.2 kJ/mol less stable than the ground **NN_s_A** conformer. The predicted IR spectrum of the **NO^-_G** conformer represents the feature at ~1500 cm^{-1} very well.

In the hydrogen-stretching region, the NN_s binding conformers uniquely contribute the intense feature at ~3550 cm^{-1}, which is associated with O–H stretching. The broad asymmetric feature observed at ~3350 cm^{-1} is associated with NH_2 asymmetric stretches contributed by both

NN_s and NO^- binding structures. Additional spectral comparisons are provided in Figure S5 for other stable low-energy NN_s conformers and in Figure S6 for other stable-low energy NO^- conformers. However, spectral misalignments (highlighted in red) indicate that these conformers do not significantly contribute to the experimental population. The high relative Gibbs energies of the N_sO and N_sO^- binding conformers, even in an aqueous polarizable continuum, indicate their lack of importance in the experiments. Spectral comparisons for these less favorable N_sO and N_sO^- modes of binding are provided in Figure S7 and Figure S8, respectively. The predicted IR spectra for all of these structures exhibit features that were not observed in the experimental IRMPD spectrum, which combined with their high relative Gibbs energies indicate their absence in the experiments. Spectral comparisons for NN_s, NO^-, NO, NsO^-, OO^- binding structures that exhibit alternative modes of sodium cation binding are provided in Figure S9. Again, spectral misalignments and high relative Gibbs energies suggest that these structures do not contribute to the experimental population. In summary, multiple stable low-energy NN_s and NO^- binding conformers of $[(Lys\text{-}H)PtCl_2+Na]^+$ were populated in the experiments. Detailed peak assignments for the spectral features observed in the IRMPD spectrum based primarily on the **NN_s_A** and **NO^-_A** conformers, but with unique contributions from the **NN_s_B**, **NO^-_G**, and **NO^-_X** conformers shown in Figure 4, are summarized in Table 4.

Structural Comparison of $[(Lys\text{-}H)PtCl_2]^-$ and $[(Lys)PtCl_2+Na]^+$. A mixture of NN_s and NO^- binding conformers of the $[(Lys\text{-}H)PtCl_2]^-$ and $[(Lys)PtCl_2+Na]^+$ complexes contribute to the experimentally measured IRMPD spectra of these complexes. The complexes differ in their states of ionization of Lys, deprotonated vs neutral, and the presence of the sodium cation, yet both complexes exhibit stable conformers with highly similar **NN_s** structures. For example, compare the **NN_s_A** and **NN_s_E** conformers of $[(Lys–H)PtCl_2]^-$ of Figure 3 to the **NN_s_B** and **NN_s_D** conformers of $[(Lys)PtCl_2+Na]^+$ of Figure 4. In contrast, the NO^- binding conformers of these complexes exhibit quite different stable conformations. A hydrogen-bonding interaction between the free carbonyl oxygen and the side chain amino group is strongly favored in $[(Lys)PtCl_2+Na]^+$, but not in $[(Lys\text{-}H)PtCl_2]^-$. The ground **NO^-_A** conformer of $[(Lys\text{-}H)PtCl_2]^-$ with the extended

side chain is predicted to be of comparable or even greater stability than other NO^- conformers that are stabilized by hydrogen bonds. In contrast, the **NO^-_X** conformer of $[(Lys)PtCl_2+Na]^+$, which is fairly similar to the **NO^-_A** of $[(Lys\text{-}H)PtCl_2]^-$ is predicted to be highly unstable in the gas phase. Despite the subtle differences in their propensities for stabilization via intramolecular hydrogen-bonding interactions, several NN_s and NO^- conformers of both $[(Lys\text{-}H)PtCl_2]^-$ and $[(Lys)PtCl_2+Na]^+$ are found to contribute to the measured IRMPD spectra. As can be seen in Figure S10, the reproduction of the spectra of these Lysplatin complexes is improved when a combination of NN_s and NO^- conformers are included as shown for a 1:1 mix of the **NN_s_E** and **NO^-_A** conformers of $[(Lys\text{-}H)PtCl_2]^-$ and 1:1 and 2:1:1 mixes of the **NN_s_A** and **NO^-_A** and **NN_s_A**, **NO^-_A**, and **NO^-_G** conformers of $[(Lys)PtCl_2+Na]^+$. In particular, the inclusion of the **NO^-_G** conformer improves the reproduction of the features in IR fingerprint region. These fits also suggest that the NN_s and NO^- binding structures are likely present in similar abundance in the experiments.

Comparison of Lysplatin Structures from IRMPD Experiments with Solid-phase Studies. Based on the measured IRMPD and theoretically predicted IR spectra for various stable modes of binding of the deprotonated and sodium cationized forms of Lysplatin, NN_s and NO^- binding structures of both complexes coexist in solution. Previous studies have reported that the mode of binding of Lys to Pt involves only the NO^- binding mode as determined by x-ray crystallography;[19,22] no evidence of NN_s conformers has previously been reported. The lack of evidence for NN_s binding conformers in these earlier works is likely attributable to the relative propensities of these complexes to crystallize out of solution. The NO^- binding conformer should be easier to crystalize due to its overall neutral charge in solution, whereas the NN_s conformers likely need lower pH to precipitate from solution than was employed in those works. As the Lysplatin complexes were formed directly from solution using the soft ionization technique of electrospray ionization in the present work, current results are not plagued by these differences in solubility/crystallization and thus reveal the previously hidden NN_s binding conformers of Lysplatin. NN_s binding conformers of Lysplatin were also not reported in the solid-phase IR

experiments as suggested by the absence of a strong C=O stretch in the IR fingerprint region.[28] However, comparison of the IRMPD spectrum of the $[(Lys\text{-}H)PtCl_2]^-$ complex measured in the present work to the solid-phase IR spectrum previously reported finds that the IR features are highly parallel. Further, the predicted IR spectra of the low-energy NN_s conformers do not exhibit a strong C=O stretch (see Figure 3) indicating that this simple criterion is insufficient for determining the presence of NN_s structures. With the ability to manipulate the charge of the complex in the mass spectrometry experiments performed here, i.e., by sodium cation adduction, evidence for a C=O stretch is readily seen and provides unequivocal evidence for the presence of NN_s binding structures of Lysplatin.

Structural Comparison of Deprotonated Lysplatin, Glyplatin and Argplatin. The measured IRMPD spectra of $[(Lys\text{-}H)PtCl_2]^-$, $[(Gly\text{-}H)PtCl_2]^-$, and $[(Arg\text{-}H)PtCl_2]^-$ are compared in Figure 2.[24,25] When the carboxylate group is deprotonated, all species exhibit highly parallel IR features. The IR band of $[(Arg\text{-}H)PtCl_2]^-$ at ~1650 cm^{-1} is slightly broader than those of $[(Lys\text{-}H)PtCl_2]^-$ and $[(Gly\text{-}H)PtCl_2]^-$ because the guanidino side chain has more C–N stretches. The predicted IR spectra of NN_s and NO^- structures for $[(Lys\text{-}H)PtCl_2]^-$ are hard to distinguish when the conformers have a free carbonyl stretch. In the case of $[(Arg\text{-}H)PtCl_2]^-$, the NN_s binding mode yields changes in the position of the C–N stretches. Thus, the NN_s binding structures have been ruled out.[25] The IRMPD spectrum of $[(Lys\text{-}H)PtCl_2]^-$ exhibits greater similarity to $[(Gly\text{-}H)PtCl_2]^-$ than $[(Arg\text{-}H)PtCl_2]^-$ in terms of the IR band at ~1200 cm^{-1}, which is associated to NH_2 wagging. Likewise, the IR band observed at ~1300 cm^{-1} for $[(Gly\text{-}H)PtCl2]^-$ is extensively broadened for $[(Lys\text{-}H)PtCl_2]^-$ and even more so for $[(Arg\text{-}H)PtCl_2]^-$ due to CH_2 wagging, CH_2 twisting, and C–C stretches of the side chains.

Structural Comparison of Sodium Cationized Lysplatin and Argplatin. The IRMPD spectra of $[(Lys)PtCl_2{+}Na]^+$ and $[(Arg)PtCl_2{+}Na]^+$ exhibit obvious differences in both the IR fingerprint and hydrogen-stretching regions. The dominant feature in the spectrum of $[(Arg)PtCl_2{+}Na]^+$ in the IR fingerprint region is associated with the C=O, C–N stretches, and NH_2 scissoring vibrational modes. The bands arising from the C–N stretches and NH_2 scissoring appear

to the blue, whereas the C=O stretch is shifted to the red. The asymmetric peak shape at ~1650 cm^{-1} arises from a combination of the vibrational modes associated with the side chain and the backbone carboxylate moiety. In contrast, the NO^- binding conformers of the $[(Lys)PtCl_2+Na]^+$ complex only exhibit an intense C=O stretch that overlaps with the red side of the intense IR feature of $[(Arg)PtCl_2+Na]^+$. The NN_s binding conformers of $[(Lys)PtCl_2+Na]^+$ exhibit a distinct IR band at ~1750 cm^{-1}. The lack of this feature in $[(Arg)PtCl_2+Na]^+$ supports the absence of NN_s binding conformers for this complex. In the hydrogen-stretching region, $[(Lys)PtCl_2+Na]^+$ exhibits an intense IR feature at ~3550 cm^{-1}, corresponding to the O–H stretch in the NN_s binding conformers. Although a similar IR feature was observed in the spectrum of $[(Arg)PtCl_2+Na]^+$, this small feature is related to the N–H asymmetric stretch of the side chain of arginine, along with several other intense N–H stretching features over the range of 3450–3600 cm^{-1} that are not observed in the spectrum of the $[(Lys)PtCl_2+Na]^+$ complex. The IR bands at ~3300 and 3350 cm^{-1} arise from the N–H stretches of the backbone amino group. In all structures populated for $[(Lys)PtCl_2+Na]^+$ and $[(Arg)PtCl_2+Na]^+$, the backbone nitrogen atom always binds to the Pt metal center. Thus, no obvious differences were observed for these N–H stretches in the measured IRMPD spectra of the $[(Lys)PtCl_2+Na]^+$ and $[(Arg)PtCl_2+Na]^+$ complexes.

Fragmentation Pathways of the Deprotonated and Sodium Cationized Lysplatin Complexes. The fragmentation behavior of Lysplatin in the gas phase may provide insight into the outstanding reactivity with DNA and RNA observed for Lysplatin as compared to the other 16 amino acid linked cisplatin complexes investigated. In previous studies of protonated, alkali metal cationized, and 18-crown-6 chelated Lys, the major fragmentation pathway observed was generally elimination of NH_3 yielding a protonated 6-membered ring pipecolic acid; H_2O loss was also observed as a minor fragmentation pathway in some cases.[31-34,60-64] The NH_3 loss has been confirmed as being derived from the side chain amino group by ^{15}N labeling experiments.[60,61] CO_2H_2 loss was observed in the fragmentation of protonated lysine but is more commonly seen as a sequential loss following elimination of NH_3. Further, the CO_2H_2 loss was proposed as a combined elimination of CO and H_2O to produce an immonium ion.[60-64]

Multiple photodissociation pathways were observed for both the $[(Lys\text{-}H)PtCl_2]^-$ and $[(Lys)PtCl_2{+}Na]^+$ complexes as summarized in Table 5; possible mechanisms for the observed fragmentation pathways of these complexes are summarized in Schemes 1 and 2, respectively, and are based on previous findings for the protonated and metal cationized Lys complexes previously investigated along with chemical intuition. The dominant fragmentation pathway of $[(Lys–H)PtCl_2]^-$ involves elimination of HCl. Cleavage of the Pt-Cl bond produces a reactive coordinatively unsaturated Pt complex that likely undergoes rearrangement to stabilize the reactive center. This fragmentation pathway is consistent with the mechanism of reactivity for cisplatin.[10,13,14] Loss of HCl was also seen in the fragmentation of the $[(Gly\text{-}H)PtCl_2]^-$ and $[(Arg\text{-}H)PtCl_2]^-$ complexes.[24,25] NH_3 loss was also observed as a minor fragmentation pathway, but only for measurements in the hydrogen-stretching region. It is also interesting to see the entire Lys ligand eliminated from the Pt metal center and complex. All other fragments observed arise from additional sequential neutral losses following elimination of HCl. The extensive sequential dissociation observed is likely partially due to the reactivity of the coordinatively undersaturated Pt center and dominantly the result of the substantial power provided by the free electron laser as these pathways are not seen in hydrogen-stretching region when activation is provided by an OPO laser system. When Lysplatin reacts with a DNA or RNA stand in solution, these sequential pathways are likely unimportant as coordination with the nucleic acid strand replaces the Pt-Cl interaction and produces a coordinatively saturated complex.

Similar behavior is observed for the $[(Lys)PtCl_2{+}Na]^+$ complex. However, while HCl loss still dominates, NH_3 loss is also competitive. Additional sequential neutral losses following elimination of HCl or NH_3 loss were also observed, with elimination of a second HCl being the most prominent. Interestingly, a greater number of dissociation pathways are observed for this complex in the hydrogen-stretching region suggesting that the neutral form of Lys is more reactive than the deprotonated form. In the case of $[(Arg)PtCl_2{+}Na]^+$, one and two HCl losses were also observed. However, HCl loss competes with elimination of H_2O rather than NH_3 for the $[(Arg)PtCl_2{+}Na]^+$ complex.[25] Several H_2 sequential loss pathways were observed in the

fragmentation of both the $[(Lys\text{-}H)PtCl_2]^-$ and $[(Lys)PtCl_2+Na]^+$ complexes, which was not observed for $[(Gly\text{-}H)PtCl_2]^+$ or protonated or metal cationized Lys complexes.[24,31-34,60-64] H_2 loss was also observed for the $[(Arg\text{-}H)PtCl_2]^-$ complex as a minor fragmentation pathway, but it was not observed for the $[(Arg)PtCl_2+Na]^+$ complex. Elimination of H_2 has previously been reported in IRMPD and tandem mass spectrometry studies of platinum complexes with methane and other alkanes.[65-73]

CONCLUSIONS

IRMPD action spectra of the deprotonated and sodium cationized forms of Lysplatin, $[(Lys\text{-}H)PtCl_2]^-$ and $[(Lys)PtCl_2+Na]^+$, were examined over the IR fingerprint and hydrogen-stretching regions using tandem mass spectrometry approaches. Elimination of HCl is observed as the dominant photodissociation pathway for both complexes, consistent with the known mechanism of reactivity of cisplatin. The measured IRMPD spectra of the $[(Lys\text{-}H)PtCl_2]^-$ and $[(Lys)PtCl_2+Na]^+$ complexes are compared with IR spectra predicted for the various stable structures and modes of binding of Lys to the Pt center level determined using the hybrid B3LYP/mDZP/def2-TZVP approach for these complexes. The calculations indicate that the most favorable mode of binding of Lys to the Pt center is NN_s, which is favored by more than 30 kJ/mol over the NO^- binding mode, and by more than 50 kJ/mol over the N_sO, N_sO^-, and OO^- modes. In spite of the large differences in stability, both NN_s and NO^- binding conformers are found to contribute to the IRMPD spectra of $[(Lys\text{-}H)PtCl_2]^-$ and $[(Lys)PtCl_2+Na]^+$, suggesting their coexistence in the ESI process. Computations performed using an aqueous polarizable continuum were pursued and indicate that the NN_s and NO^- conformers are of comparable stability in aqueous solution, and thus explain the presence of the less stable gas-phase NO^- conformers in the experiments. Present results indicated that changes in the local environment do not alter the modes of binding of Lys to the Pt center, confirming that the Pt-Lys interactions are preserved under different pH and ionic strength environments. The presence of NN_s conformers in the experiments, which were not observed for the analogous Glyplatin and Argplatin complexes previously

investigated suggest that these structures may be responsible for the outstanding reactivity observed for Lysplatin.

ASSOCIATED CONTENT

Supporting Information

The Supporting Information is available free of charge at https://pubs/acs.org/doi/***

Figures comparing the stable low-energy B3LYP/mDZP/def2-TZVP conformations of the $[(Lys\text{-}H)PtCl_2]^-$ and $[(Lys)PtCl_2+Na]^+$ complexes and their relative Gibbs energies at 298 K; comparisons of the experimental IRMPD action spectra of the $[(Lys\text{-}H)PtCl_2]^-$ and $[(Lys)PtCl_2+Na]^+$ complexes with the B3LYP/mDZP/def2-TZVP optimized structures and calculated linear IR spectra predicted for stable low-energy conformers as a function of the Pt binding modes, NN_s, NO^-, N_sO, N_sO^-, and OO^- binding modes (PDF).

AUTHOR INFORMATION

Corresponding Author

Mary T. Rodgers - *Department of Chemistry, Wayne State University, Detroit, Michigan, 48202, United States*; orcid.org/0000-0002-5614-0948; Phone (313) 577-2431; Email: mrodgers@chem.wayne.edu

Authors

C. C. He - *Department of Chemistry, Wayne State University, Detroit, Michigan, 48202, United States*; orcid.org/0000-0002-0500-1526

L. A. Hamlow - *Department of Chemistry, Wayne State University, Detroit, Michigan, 48202, United States*; orcid.org/0000-0002-7988-5117

H. A. Roy - *Department of Chemistry, Wayne State University, Detroit, Michigan, 48202, United States*; orcid.org/0000-0002-9128-5245

Zachary J. Devereaux - *Department of Chemistry, Wayne State University, Detroit, Michigan, 48202, United States*; orcid.org/0000-0002-8385-3492

M. A. Hasan - *Department of Chemistry, Wayne State University, Detroit, Michigan, 48202, United States*; orcid.org/0000-0001-7651-6140

E. Israel - *Department of Chemistry, Wayne State University, Detroit, Michigan, 48202, United States*; orcid.org/0000-0002-5563-9720

N. A. Cunningham - *Department of Chemistry, Wayne State University, Detroit, Michigan, 48202, United States*; orcid.org/0000-0003-2145-9032

J. Martens – *Radboud University, Institute for Molecules and Materials, FELIX Laboratory, Nijmegen, The Netherlands;* orcid.org/0000-0001-9537-4117

G. Berden – *Radboud University, Institute for Molecules and Materials, FELIX Laboratory, Nijmegen, The Netherlands;* orcid.org/0000-0003-1500-922X

J. Oomens – *Radboud University, Institute for Molecules and Materials, FELIX Laboratory, Nijmegen, The Netherlands;* orcid.org/0000-0002-2717-1278

ACKNOWLEDGEMENTS

This work was financially supported by the National Science Foundation, under Grants OISE-0730072, OISE-1357787 (for the IRMPD measurements and international travel), DBI-0922819 (for the Bruker amaZon ETD QITMS employed in this work), CHE-1709789. C.C.H., L.A.H., H.A.R., and Z.J.D. thank Wayne State University for support via Thomas C. Rumble Graduate Research Fellowships. We thank Wayne State University C&IT for the computational resources and support. We acknowledge the Nederlandse Organisatie voor Wetenschappelijk Onderzoek (NWO) for support of the FELIX Laboratory. The skillful assistance of the FELIX staff is gratefully acknowledged. Thanks to B. Kimutai and C.S. Chow for providing the Lysplatin examined in this work.

REFERENCES

1. Lippert, B., *Cisplatin: Chemistry and Biochemistry of a Leading Anticancer Drug*; Wiley-VCH: Weinheim, Germany, 1999.
2. Rosenberg, B. Platinum Complexes for Treatment of Cancer. *Interdiscipl. Sci. Rev.* **1978**, *3*, 134-147.
3. Rosenberg, B.; VanCamp, L.; Krigas, T. Inhibition of Cell Division in Escherichia Coli by Electrolysis Products from a Platinum Electrode. *Nature* **1965**, *205*, 698-699.
4. Rosenberg, B.; VanCamp, L.; Trosko, J. E.; Mansour, V. H. Platinum Compounds - A New Class of Potent Antitumour Agents. *Nature* **1969**, *222*, 385-386.
5. Kartalou, M.; Essigmann, J. M. Recognition of Cisplatin Adducts by Cellular Proteins. *Mutat. Res.-Fund. Mol. M.* **2001**, *478*, 1-21.
6. McWhinney, S. R.; Goldberg, R. M.; McLeod, H. L. Platinum Neurotoxicity Pharmacogenetics. *Mol. Cancer Ther.* **2009**, *8*, 10-16.
7. Jamieson, E. R.; Lippard, S. J. Structure, Recognition, and Processing of Cisplatin-DNA Adducts. *Chem. Rev.* **1999**, *99*, 2467-2498.
8. Hostetter, A. A.; Chapman, E. G.; DeRose, V. J. Rapid Cross-Linking of an RNA Internal Loop by the Anticancer Drug Cisplatin. *J. Am. Chem. Soc.* **2009**, *131*, 9250-9257.
9. Kelland, L. R.; Sharp, S. Y.; O'Neill, C. F.; Raynaud, F. I.; Beale, P. J.; Judson, I. R. Mini-Review: Discovery and Development of Platinum Complexes Designed to Circumvent Cisplatin Resistance. *J. Inorg. Biochem.* **1999**, *77*, 111-115.
10. Galanski, M.; Jakupec, M. A.; Keppler, B. K. Update of the Preclinical Situation of Anticancer Platinum Complexes: Novel Design Strategies and Innovative Analytical Approaches. *Curr. Med. Chem.* **2005**, *12*, 2075-2094.
11. Holford, J.; Sharp, S. Y.; Murrer, B. A.; Abrams, M.; Kelland, L. R. In Vitro Circumvention of Cisplatin Resistance by the Novel Sterically Hindered Platinum Complex AMD473. *Brit. J. Cancer* **1998**, *77*, 366-373.
12. Reedijk, J. Why Does Cisplatin Reach Guanine-N7 with Competing S-Donor Ligands Available in the Cell? *Chem. Rev.* **1999**, *99*, 2499-2510.
13. Cleare, M. J.; Hoeschele, J. D. Studies on the Antitumor Activity of Group VIII Transition Metal Complexes, Part I. Platinum(II) Complexes. *Bioinorg. Chem.* **1973**, *2*, 187-210.
14. Cleare, M. J.; Hoeschele, J. D. Antitumor Platinum Compounds - Relationship Between Structure and Activity. *Platin. Met. Rev.* **1973**, *17*, 2-13.
15. Paciotti, R.; Corinti, D.; De Petris, A.; Ciavardini, A.; Piccirillo, S.; Coletti, C.; Re, N.; Maitre, P.; Bellina, B.; Barran, P.; Chiavarino, B.; Crestoni, M. E.; Fornarini, S. Cisplatin and Transplatin Interaction with Methionine: Bonding Motifs Assayed by Vibrational Spectroscopy in the Isolated Ionic Complexes. *Phys. Chem. Chem. Phys*. **2017**, *19*, 26697-26707.
16. Paciotti, R.; Corinti, D.; Maitre, P.; Coletti, C.; Re, N.; Chiavarino, B.; crestoni, M. e.; fornarini, S. From Preassociation to Chelation: a Survery of Cisplatin Interaction with Methionine at Molecule Level by IR Ion Spectrsocopy and Computations. *J. Am. Soc. Mass Spectrom*. **2021**, *32*, 2206-2217.
17. Corinti, D.; De Petris, A.; Coletti, C.; Re, N.; Chiavariano, B.; Crestoni, M. E.; Fornarini, S. Cisplatin Primary Complex with L-Histidine Target Revealed by IR Multiple Photon Dissociation (IRMPD) Spectroscopy. *ChemPhysChem* **2017**, *18*, 318-325.

18. Nelson, D. L.; Cox, M. M., *Lehninger Principles of Biochemistry*, Seventh ed.; W. H. Freeman and Company: New York, NY, 2017, p 1-1328.
19. Sandman, K. E.; Fuhrmann, P.; Lippard, S. J. A Mechanism-Based, Solution-Phase Method for Screening Combinatorial Mixtures of Potential Platinum Anticancer Drugs. *J. Biol. Inorg. Chem.* **1998**, *3*, 74-80.
20. Rijal, K.; Bao, X.; Chow, C. S. Amino Acid-Linked Platinum(II) Analogues Have Altered Specificity for RNA Compared to Cisplatin. *Chem. Commun.* **2014**, *50*, 3918-3920.
21. Rijal, K.; Chow, C. S. A New Role for Cisplatin: Probing Ribosomal RNA Structure. *Chem. Commun.* **2009**, 107-109.
22. Ziegler, C. J.; Sandman, K. E.; Liang, C. H.; Lippard, S. J. Toxicity of Platinum(II) Amino Acid (N,O) Complexes Parallels Their Binding to DNA as Measured in a New Solid Phase Assay Involving a Fluorescent HMG1 Protein Construct Readout. *J. Biol. Inorg. Chem.* **1999**, *4*, 402-411.
23. Dalla Via, L.; Gia, O.; Magno, S. M.; Dolmella, A.; Marton, D.; Di Noto, V. Synthesis, Characterization and Biological Activity of Platinum(II) Complexes with L- and D-Ornithine Ligands. *Inorg. Chim. Acta* **2006**, *359*, 4197-4206.
24. He, C. C.; Kimutai, B.; Bao, X.; Hamlow, L.; Zhu, Y.; Strobehn, S. F.; Gao, J.; Berden, G.; Oomens, J.; Chow, C. S.; Rodgers, M. T. Evaluation of Hybrid Theoretical Approaches for Structural Determination of a Glycine-Linked Cisplatin Derivative via Infrared Multiple Photon Dissociation (IRMPD) Action Spectroscopy. *J. Phys. Chem. A* **2015**, *119*, 10980-10987.
25. He, C. C.; Hamlow, L. A.; Kimutai, B.; Roy, H. A.; Devereaux, Z. J.; Cunningham, N. A.; Martens, J. K.; Berden, G.; Oomens, J.; Chow, C. S.; Rodgers, M. T. Structural Determination of Arginine-Linked Cisplatin Complexes via IRMPD Action Spectroscopy: Arginine Binds to Platinum via NO^- Binding Mode. *Phys. Chem. Chem. Phys.* **2021**, *23*, 21959-21971.
26. Altman, J.; Wilchek, M. Platinum(II) Complexes with Diaminopropionic Acid as Oxygen-Bound Unidentate, Nitrogen Oxygen and Nitrogen Nitrogen Chelate Complexes. *Inorg. Chim. Acta* **1985**, *101*, 171-173.
27. Altman, J.; Wilchek, M.; Warshawsky, A. Platinum(II) Complexes with 2,4-Diaminobutyric Acid, Ornithine, Lysine and 4,5-Diaminovaleric Acid. *Inorg. Chim. Acta* **1985**, *107*, 165-168.
28. Bino, A.; Cohen, S.; Altman, J.; Wilchek, M. The Crystal and Molecular-Structures of Dichloro[N,O-(D,L)-Diaminopropionic Acid] Platinum(II) and Dichloro[N,O-(L)-Lysine] Platinum(II) Monohydrate. *Inorg. Chim. Acta* **1988**, *147*, 99-102.
29. Noji, M.; Hanamura, S.; Suzuki, K.; Tashiro, T.; Kidani, Y. Antitumor-Activity of Pt(II) Complexes Containing Diaminocarboxylates and Their Ester Derivatives. *Chem. Pharm. Bull.* **1986**, *34*, 2487-2493.
30. Zorko, M.; Langel, U. Cell-Penetrating Peptides: Mechanism and Kinetics of Cargo Delivery. *Adv. Drug. Deliver. Rev.* **2005**, *57*, 529-545.
31. Lemoff, A. S.; Bush, M. F.; O'Brien, J. T.; Williams, E. R. Structures of Lithiated Lysine and Structural Analogues in the Gas Phase: Effects of Water and Proton Affinity on Zwitterionic Stability. *J. Phys. Chem. A* **2006**, *110*, 8433-8442.
32. Bush, M. F.; Forbes, M. W.; Jockusch, R. A.; Oomens, J.; Polfer, N. C.; Saykally, R. J.; Williams, E. R. Infrared Spectroscopy of Cationized Lysine and ε-N-Methyllysine in the Gas Phase: Effects of Alkali-Metal Ion Size and Proton Affinity on Zwitterion Stability. *J. Phys. Chem. A* **2007**, *111*, 7753-7760.
33. Bush, M. F.; Oomens, J.; Williams, E. R. Proton Affinity and Zwitterion Stability: New Results from Infrared Spectroscopy and Theory of Cationized Lysine and Analogues in the Gas Phase. *J. Phys. Chem. A* **2009**, *113*, 431-438.

34. Clark, A. A.; Yang, B.; Rodgers, M. T.; Armentrout, P. B. Experimental and Computational Study of the Group 1 Metal Cation Chelates with Lysine: Bond Dissociation Energies, Structures, and Structural Trends. *J. Phys. Chem. B* **2019**, *123*, 1983-1997.
35. Kimutai, B., "Non-Canonical Targets, Reaction Kinetics, and Cellular Potency of Amino Acid-Linked Platinum(II) Compounds" (2020). *Wayne State University Dissertations*, 2360. https://digitalcommons.wayne.edu/oa_dissertations/2360
36. Bao, X., "Synthesis, Characterization, and RNA Reactivity of Amino-Acid-Linked Cisplatin Analogues" (2015). *Wayne State University Dissertations*, 1115. https://digitalcommons.wayne.edu/oa_dissertations/1115
37. Oepts, D.; van der Meer, A. F. G.; van Amersfoort, P. W. The Free-Electron-Laser User Facility FELIX. *Infrared Phys. Techn.* **1995**, *36*, 297-308.
38. Martens, J.; Berden, G.; Gebhardt, C.R.; Oomens, J. Infrared Ion Spectroscopy in a Modified Quadrupole Ion Trap Mass Spectrometer at the FELIX Free Electron Laser Laboratory. Rev. Scientific Instruments **2016**, *87*, 103108 *Rev. Sci. Instrum.* **2016**, *87*, 103108.
39. Martens, J.; Berden, G.; Oomens, J. Structures of Fluoranthene Reagent Anions Used in Electron Transfer Dissociation and Proton Transfer Reaction Tandem Mass Spectrometry. *Anal. Chem.* **2016**, *88*, 6126-6129.
40. Martens, J.; Grzetic, J.; Berden, G.; Oomens, J. Structural Identification of Electron Transfer Dissociation Products in Mass Spectrometry using Infrared Ion Spectroscopy. *Nat. Commun.* **2016**, *7*, 11754.
41. Hamlow, L. A.; Zhu, Y.; Devereaux, Z. J.; Cunningham, N. A.; Berden, G.; Oomens, J.; Rodgers, M. T. Modified Quadrupole Ion Trap Mass Spectrometer for Infrared Ion Spectroscopy: Application to Protonated Thiated Uridines. *J. Am. Soc. Mass Spectrom.* **2018**, *29*, 2125-2137.
42. Berden, G.; Derksen, M.; Jouthujis, K.J.; Martens, J.; Oomens, J. An Automatic Variable Laser Attenuator for IRMPD Spectroscopy and Analysis of Power-Dependence in Fragmentation Spectra. *Int. J. Mass Spectrom*. **2019**, *443*, 1-8.
43. He, C. C., "Characterization of Protonated Modified Nucleosides and Amino Acid-Linked Cisplatin Analogues Using Tandem Mass Spectrometry Complemented by Theoreticical Approaches" (2018). *Wayne State University Dissertation*s, 2103. https://digitalcommons.wayne.edu/oa_dissertations/2103
44. *Gaussian 09*, Revision C01, Frisch, M. J.; Trucks, G. W.; Schlegel, H. B.; Scuseria, G. E.; Robb, M. A.; Cheeseman, J. R.; Scalmani, G.; Barone, V.; Mennucci, B.; Petersson, G. A., et al., Gaussian, Inc., Wallingford, CT, USA, 2009.
45. Feller, D. The Role of Databases in Support of Computational Chemistry Calculations. *J. Comput. Chem.* **1996**, *17*, 1571-1586.
46. Schuchardt, K. L.; Didier, B. T.; Elsethagen, T.; Sun, L. S.; Gurumoorthi, V.; Chase, J.; Li, J.; Windus, T. L. Basis Set Exchange: A Community Database for Computational Sciences. *J. Chem. Inf. Model.* **2007**, *47*, 1045-1052.
47. Wysokinski, R.; Michalska, D. The Performance of Different Density Functional Methods in the Calculation of Molecular Structures and Vibrational Spectra of Platinum(II) Antitumor Drugs: Cisplatin and Carboplatin. *J. Comput. Chem.* **2001**, *22*, 901-912.
48. Wolinski, K.; Hinton, J. F.; Wishart, D. S.; Sykes, B. D.; Richards, F. M.; Pastone, A.; Saudek, V.; Ellis, P. D.; Maciel, G. E.; McIver, J. W., Jr., et al., Hypercube, Inc., Gainsville, FL, 2004.
49. Bertsimas, D.; Tsitsiklis, J. Simulated Annealing. *Stat. Sci.* **1993**, *8*, 10-15.
50. Allinger, N. L. Conformational Analysis. 130. MM2. A Hydrocarbon Force Field Utilizing V_1 and V_2 Torsional Terms. *J. Am. Chem. Soc.* **1977**, *99*, 8127-8134.

51. Cundari, T. R.; Fu, W.; Moody, E. W.; Slavin, L. L.; Snyder, L. A.; Sommerer, S. O.; Klinckman, T. R. Molecular Mechanics Force Field for Platinum Coordination Complexes. *J. Phys. Chem.-US* **1996**, *100*, 18057-18064.
52. Cundari, T. R.; Fu, W. T. Conformational Analysis of Platinum Antitumor Drugs. *J. Mol. Struc.-THEOCHEM* **1998**, *425*, 51-60.
53. Wu, R. R.; Yang, B.; Berden, G.; Oomens, J.; Rodgers, M. T. Gas-Phase Conformations and Energetics of Protonated 2'-Deoxyguanosine and Guanosine: IRMPD Action Spectroscopy and Theoretical Studies. *J. Phys. Chem. B* **2014**, *118*, 14774-14784.
54. Wu, R. R.; Yang, B.; Berden, G.; Oomens, J.; Rodgers, M. T. Gas-Phase Conformations and Energetics of Protonated 2'-Deoxyadenosine and Adenosine: IRMPD Action Spectroscopy and Theoretical Studies. *J. Phys. Chem. B* **2015**, *119*, 2795-2805.
55. Wu, R. R.; Yang, B.; Frieler, C. E.; Berden, G.; Oomens, J.; Rodgers, M. T. N3 and O2 Protonated Tautomeric Conformations of 2'-Deoxycytidine and Cytidine Coexist in the Gas Phase. *J. Phys. Chem. B* **2015**, *119*, 5773-5784.
56. Wu, R. R.; Yang, B.; Frieler, C. E.; Berden, G.; Oomens, J.; Rodgers, M. T. Diverse Mixtures of 2,4-Dihydroxy Tautomers and O4 Protonated Conformers of Uridine and 2'-Deoxyuridine Coexist in the Gas Phase. *Phys. Chem. Chem. Phys.* **2015**, *17*, 25978-25988.
57. Wu, R. R.; Yang, B.; Frieler, C. E.; Berden, G.; Oomens, J.; Rodgers, M. T. 2,4-Dihydroxy and O2 Protonated Tautomers of dThd and Thd Coexist in the Gas Phase: Methylation Alters Protonation Preferences versus dUrd and Urd. *J. Am. Soc. Mass Spectrom.* **2016**, *27*, 410-421.
58. Wu, R. R.; He, C. C.; Hamlow, L. A.; Nei, Y.-w.; Berden, G.; Oomens, J.; Rodgers, M. T. Protonation Induces Base Rotation of Purine Nucleotides pdGuo and pGuo. *Phys. Chem. Chem. Phys.* **2016**, *18*, 15081-15090.
59. Wu, R. R.; He, C. C.; Hamlow, L. A.; Nei, Y.-w.; Berden, G.; Oomens, J.; Rodgers, M. T. N3 Protonation Induces Base Rotation of 2'-Deoxyadenosine-5'-Monophosphate and Adenosine-5'-Monophosphate. *J. Phys. Chem. B* **2016**, *120*, 4616-4624.
60. Milne, G. W. A.; Vestal, M. L.; Fales, H. M. Chemical Ionization Mass Spectrometry of Complex Molecules. IV. Amino Acids. *J. Am. Chem. Soc.* **1969**, *92*, 5170-5175.
61. Dookeran, N. N.; Yalcin, T.; Harrison, A. G. Fragmentation Reactions of Protonated α-Amino Acids. *J. Mass Spectrom.* **1996**, *31*, 500-508.
62. Yalcin, T.; Harrison, A. G. Ion Chemistry of Protonated Lysine Derivatives. *J. Mass Spectrom.* **1996**, *31*, 1237-1243.
63. Rogalewicz, F.; Hoppilliard, Y.; Ohanessian, G. Fragmentation Mechanisms of α-Amino Acids Protonated under Electrospray Ionization: A Collisional Activation and Ab Initio Theoretical Study. *Int. J. Mass Spectrom.* **2000**, *195*, 565-590.
64. Chen, Y.; Rodgers, M. T. Structural and Energetic Effects in the Molecular Recognition of Amino Acids by 18-Crown-6. *J. Am. Chem. Soc.* **2012**, *134*, 5863-5875.
65. Wheeler, O. W.; Salem, M.; Gao, A.; Bakker, J. M.; Armentrout, P. B. Activation of C-H Bonds in Pt^+ + x CH_4 Reactions, where x=1-4: Identification of the Platinum Dimethyl Cation. *J. Phys. Chem. A* **2016**, *120*, 6216-6227.
66. Lapoutre, V. J. F.; Redlich, B.; van der Meer, A. F. G.; Oomens, J.; Bakker, J. M.; Sweeney, A.; Mookherjee, A.; Armentrout, P. B. Structures of the Dehydrogenation Products of Methane Activation by 5d Transition Metal Cations. *J. Phys. Chem. A* **2013**, *117*, 4115-4126.
67. Koszinowski, K.; Schroder, D.; Schwarz, H. Reactions of Platinum-Carbene Clusters $Pt_nCH_2^+$ (n=1-5) with O_2, CH_4, NH_3, and H_2O: Coupling Processes versus Carbide Formation. *Organometallics* **2003**, *22*, 3809-3819.

68. Koszinowski, K.; Schroder, D.; Schwarz, H. Reactivity of Small Cationic Platinum Clusters. *J. Phys. Chem. A* **2003**, *107*, 4999-5006.
69. Zhang, X. G.; Liyanage, R.; Armentrout, P. B. Potential Energy Surface for Activation of Methane by Pt^+: A Combined Guided Ion Beam and DFT Study. *J. Am. Chem. Soc.* **2001**, *123*, 5563-5575.
70. Irikura, K. K.; Beauchamp, J. L. Electronic-Structure Considerations for Methane Activation by 3rd-Row Transition-Metal Ions. *J. Phys. Chem.* **1991**, *95*, 8344-8351.
71. Irikura, K. K.; Beauchamp, J. L. Methane Oligomerization in the Gas-Phase by 3rd-Row Transition-Metal Ions. *J. Am. Chem. Soc.* **1991**, *113*, 2769-2770.
72. Adlhart, C.; Uggerud, E. Mechanisms for the Dehydrogenation of Alkanes on Platinum: Insights Gained from the Reactivity of Gaseous Cluster Cations, Pt_n^+ n=1-21. *Chem. Eur. J.* **2007**, *13*, 6883-6890.
73. Adlhart, C.; Uggerud, E. Reactions of Platinum Clusters $Pt_n^{\pm}$, n=1-21, with CH_4: To React or Not to React. *Chem. Commun.* **2006**, 2581-2582.

Table 1. Relative Gibbs Energies of Representative Stable Low-Energy Conformers of $[(\text{Lys-H})PtCl_2]^-$ at 298 K in kJ/mol.[a]

Conformer	ΔG_{298}	ΔG_{298}(water)
NN_s_A	**0.0**	0.8
NN_s_C	20.0	6.9
NN_s_E	24.5	**0.0**
NN_s_G	29.7	9.7
NO^-_A	32.9	13.6
NO^-_E	35.3	10.0[b]
NO^-_F	34.6	9.9
NO^-_G	35.5	10.4
NO^-_I	36.1	7.5[b]
NO^-_L	36.9	12.0
NO^-_Q	38.5	16.1
NO^-_AC	42.3	11.7[b]
N_sO^-_A	41.6	25.0
NO^-_AX	49.6	27.3
N_sO^-_C	45.0	33.2
N_sO^-_L	57.6	32.0
N_sO^-_O	59.0	45.2
N_sO^-_AB	79.2	48.1
N_sO^-_AC	82.1	56.7
OO^-_A	97.6	92.0

[a]See Figure S1 for the B3LYP/6-311+G(d,p) optimized geometries of low-energy these conformers. Relative stabilities are provided in vacuo and in an aqueous polarizable continuum. [b]Application of implicit solvation produced structural changes involving loss of one hydrogen-bonding interaction.

Table 2. Relative Gibbs Energies of Representative Stable Low-Energy Conformers of $[(Lys)PtCl_2+Na]^+$ at 298 K in kJ/mol.[a]

Conformer	ΔG_{298}	ΔG_{298}(water)
NN_s_A	**0.0**	**0.0**
NN_s_B	1.2	10.1
NN_s_D	4.1	1.6
NN_s_E	4.2	2.8
NN_s_O	18.1	12.9[b]
NN_s_S	20.8	18.0
NN_s_OCl_bCl_s_A	22.7	16.7
NO^-_A	32.6	7.6[b]
NO^-_D	37.6	3.2
NO^-_F	38.4	16.9[b]
NO^-_G	38.8	7.5
NO^-_H	39.2	0.2
NO^-_OCl_b_A	46.5	7.8
N_sO_A	50.4	57.7
N_sO^-_A	54.5	28.8
N_sO_C	55.3	56.2
NN_s_OCl_s_A	56.5	13.3
N_sO_D	59.4	67.7
NO_A	59.5	62.6
N_sO^-_B	59.7	25.8
NO_$N_sCl_bCl_O$_A	65.4	71.8
N_sO_I	65.4	72.1
N_sO_K	66.5	75.9
N_sO^-_J	84.8	53.8[b]
N_sO^-_$OOCl_s$_A	85.8	27.3
N_sO^-_L	85.9	40.4
N_sO^-_M	86.9	50.5
N_sO^-_OCl_s_A	87.0	16.6
NN_s_OO_A	89.1	14.1[c]
NO^-_R	101.0	28.7
NO^-_S	109.6	24.8
OO^-_A	113.9	94.8
NO^-_U	120.3	20.8
NO^-_X	140.3	3.9
NN_s_O_A	152.0	19.2
NO_N_s_A	248.6	61.8
NO_N_sO_A	273.7	79.5[c]

[a]See Figure S1 for the B3LYP/6-311+G(d,p) optimized geometries of low-energy these conformers. Relative stabilities are provided in vacuo and in an aqueous polarizable continuum.
[b]Application of implicit solvation resulted in a significant change in or loss of one hydrogen-bonding interaction.
[c] Major structural change, Na^+ binding mode changes from bidentate to monodentate.

Table 3. Vibrational Band Assignments for the $[(Lys\text{-}H)PtCl_2]^-$ Complex Based on Conformers **NN_s_E** and **NO^-_A**.[a]

Experimental Band (cm^{-1})	**NN_s_E**	**NO^-_A**
1046	–	NH_2 wagging
1157	NH_2 wagging	–
1242–1383	C–H wagging/twisting	C–H wagging/twisting
1581	N_sH_2 scissoring	NH_2 scissoring
1608	NH_2 scissoring	N_sH_2 scissoring
1675	C=O stretch	C=O stretch
3354	N_sH_2 asymmetric stretching	N_sH_2 asymmetric stretching

[a]A scaling factor of 0.970 was used in the fingerprint region (FEL), whereas a scaling factor of 0.957 was used in the hydrogen-stretching region (OPO). See Figure 1 for atom designations.

Table 4. Vibrational Band Assignments for the $[(Lys)PtCl_2+Na]^+$ Complex Based Primarily on the **NN_s_A** and **NO^-_A** Conformers.[a]

Experimental Band (cm^{-1})	**NN_s_A**	**NO^-_A**
1113	–	NH_2/N_sH_2 wagging/twisting
1134	CH_2 twisting/C–O(H) stretch	
1200	NH_2/N_sH_2 wagging/twisting	
1382	CH_2 wagging	CH_2 wagging
1436	CH_2 scissoring	CH_2 scissoring
1500	–	N_sH_2 scissoring[b]
1515	–	N_sH_2 scissoring
1579	NH_2/N_sH_2 scissoring	C=O stretch
1612	–	NH_2/N_sH_2 scissoring
1709	–	C=O stretch[c]
1727	C=O stretch[c]	
1761	C=O stretch	–
3296	NH_2/N_sH_2 symmetric stretch	NH_2/N_sH_2 symmetric stretch
3324	–	N_sH_2 asymmetric stretch[d]
3344	NH_2/N_sH_2 asymmetric stretch	–
3360	–	NH_2/N_sH_2 asymmetric stretch
3564	O-H stretch	–

[a]A scaling factor of 0.970 was used in the fingerprint region (FEL), whereas a scaling factor of 0.960 was used in the hydrogen-stretching region (OPO). [b]Vibrational mode from conformer **NO^-_G**. [c]Vibrational mode from conformer **NN_s_B**. [d] Vibrational mode from conformer **NO^-_X**.

Table 5. Fragment Ions Observed upon IRMPD of Lysplatin Complexes in the IR Fingerprint (FEL) and Hydrogen-Stretching (OPO) Regions.[a]

Precursor/Product Ion	m/z (Exact)	m/z (FEL)	m/z (OPO)	Neutral Losses
$[(Lys\text{-}H)PtCl_2]^-$				
$C_6H_{13}N_2O_2Cl_2Pt$	410.0002	409.7	410.001	
$C_6H_{10}NO_2Cl_2Pt$	392.9736		392.973	NH_3
$C_6H_{12}N_2O_2ClPt$	374.0235	373.8	374.024	HCl
$C_6H_{10}N_2O_2ClPt$	372.0079	371.7		$HCl+H_2$
$C_6H_9NO_2ClPt$	356.9970	356.7		$HCl+NH_3$
$C_6H_7NO_2ClPt$	354.9813	354.8		$HCl+H_2+NH_3$
$C_6H_{11}N_2O_2Pt$	338.0468	337.8		2HCl
$C_6H_9N_2O_2Pt$	336.0312	335.8		$2HCl+H_2$
$C_5H_{12}N_2ClPt$	330.0337	329.8		$HCl+CO_2$
$C_5H_{10}N_2ClPt$	328.0180	327.7		$HCl+CO_2+H_2$
$C_5H_8N_2ClPt$	326.0024	325.7		$HCl+CO_2+2H_2$
C_5H_9NClPt	313.0071	312.7		$HCl+NH_3+CO_2$
C_5H_7NClPt	310.9915	310.7		$HCl+NH_3+CO_2+H_2$
C_5H_5NClPt	308.9758	308.7		$HCl+NH_3+CO_2+2H_2$
$C_5H_9N_2Pt$	292.0413	291.7		$2HCl+CO_2H_2$
HCl_2Pt	265.9103	265.5		Lys–2H
CHNClPt	256.9445	256.5		$HCl+NH_3+CO_2+2H_2+C_4H_4$
H_2ClPt	231.9493	231.4		HCl+(Lys–4H)
$[(Lys)PtCl_2+Na]^+$				
$C_6H_{14}N_2O_2Cl_2PtNa$	433.9978	433.8	433.9	
$C_6H_{11}NO_2Cl_2PtNa$	416.9712	416.8	416.9	NH_3
$C_6H_{13}N_2O_2ClPtNa$	398.0211	397.8	397.9	HCl
$C_6H_{10}NO_2ClPtNa$	380.9946	380.8	381.0	$HCl + NH_3$
$C_6H_{12}N_2O_2PtNa$	362.0444	361.9	362.0	2HCl
$C_6H_{10}N_2O_2PtNa$	360.0288	359.9		$2HCl + H_2$
$C_6H_8N_2O_2PtNa$	358.0131	357.8		$2HCl + 2H_2$
$C_6H_9NO_2PtNa$	345.0179	344.8	345.0	$2HCl + NH_3$
$C_5H_{10}N_2PtNa$	316.0390	315.8		$2HCl + CO_2H_2$

[a]Note that the differences in the m/z of the precursor and product ions are associated with limitations on the m/z accuracy of the QIT MS and FT-ICR MS instruments.

Figure Captions

Figure 1. Chemical structures of cisplatin, lysine, and Lysplatin. The *cis* bidentate NO^- and NN_s binding modes of Lysplatin, the most favorable modes of binding of the zwitterionic and nonzwitterionic forms of Lys to the Pt center, are shown.

Figure 2. Experimental IRMPD spectra of the $[(Lys\text{-}H)PtCl_2]^-$ and $[(Lys)PtCl_2+Na]^+$ complexes over the IR fingerprint (600–1850 cm^{-1}) and hydrogen-stretching (3200–3650 cm^{-1}) regions. The IRMPD spectra of the $[(Gly\text{-}H)PtCl_2]^-$, $[(Arg\text{-}H)PtCl_2]^-$, and $[(Arg)PtCl_2+Na]^+$ complexes previously reported are overlaid in grey and black for comparison and are taken from references 21 and 22.

Figure 3. Comparison of the experimental IRMPD spectrum of $[(Lys\text{-}H)PtCl_2]^-$ with theoretical IR spectra predicted for selected stable low-energy NN_s and NO^- binding conformers along with their optimized structures and relative B3LYP/mDZP/def2-TZVP Gibbs energies at 298 K; values in black are for the isolated species, whereas values in red are computed in aqueous polarizable continuum.

Figure 4. Comparison of the experimental IRMPD spectrum of $[(Lys)PtCl_2+Na]^+$ with theoretical IR spectra predicted for select stable low-energy NN_s and NO^- binding conformers along with their optimized structures and relative B3LYP/mDZP/def2-TZVP Gibbs energies at 298 K; values in black are for the isolated species, whereas values in red are computed in aqueous polarizable continuum.

Scheme 1. Proposed fragmentation pathways of the $[(Lys\text{-}H)PtCl_2]^-$ complex. Reaction pathways resulting in elimination of HCl are described by the green arrows, NH_3 by blue arrows, H_2CO_2 by red arrows, Lys by yellow arrows, and H_2 by black arrows.

Scheme 2. Proposed fragmentation pathways of the $[(Lys)PtCl_2+Na]^+$ complex. Reaction pathways resulting in elimination of HCl are described by the green arrows, NH_3 by blue arrows, H_2CO_2 by red arrows, and H_2 by black arrows.

Figure 1.

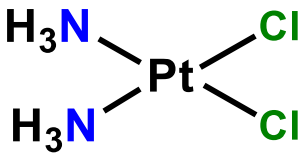

Cisplatin

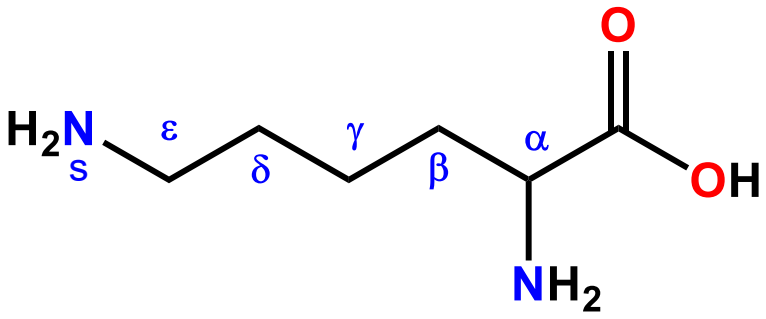

Lysine ($C_6H_{14}N_2O_2$)

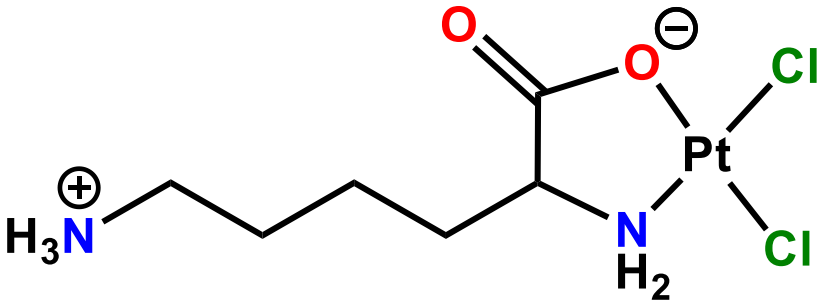

NO^- Binding Mode

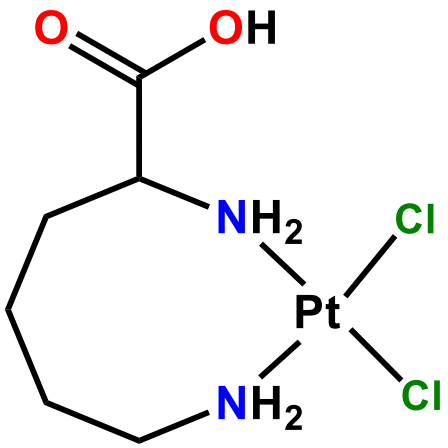

NN_s Binding Mode

Lysine-Linked Cisplatin (Lysplatin)

Figure 2.

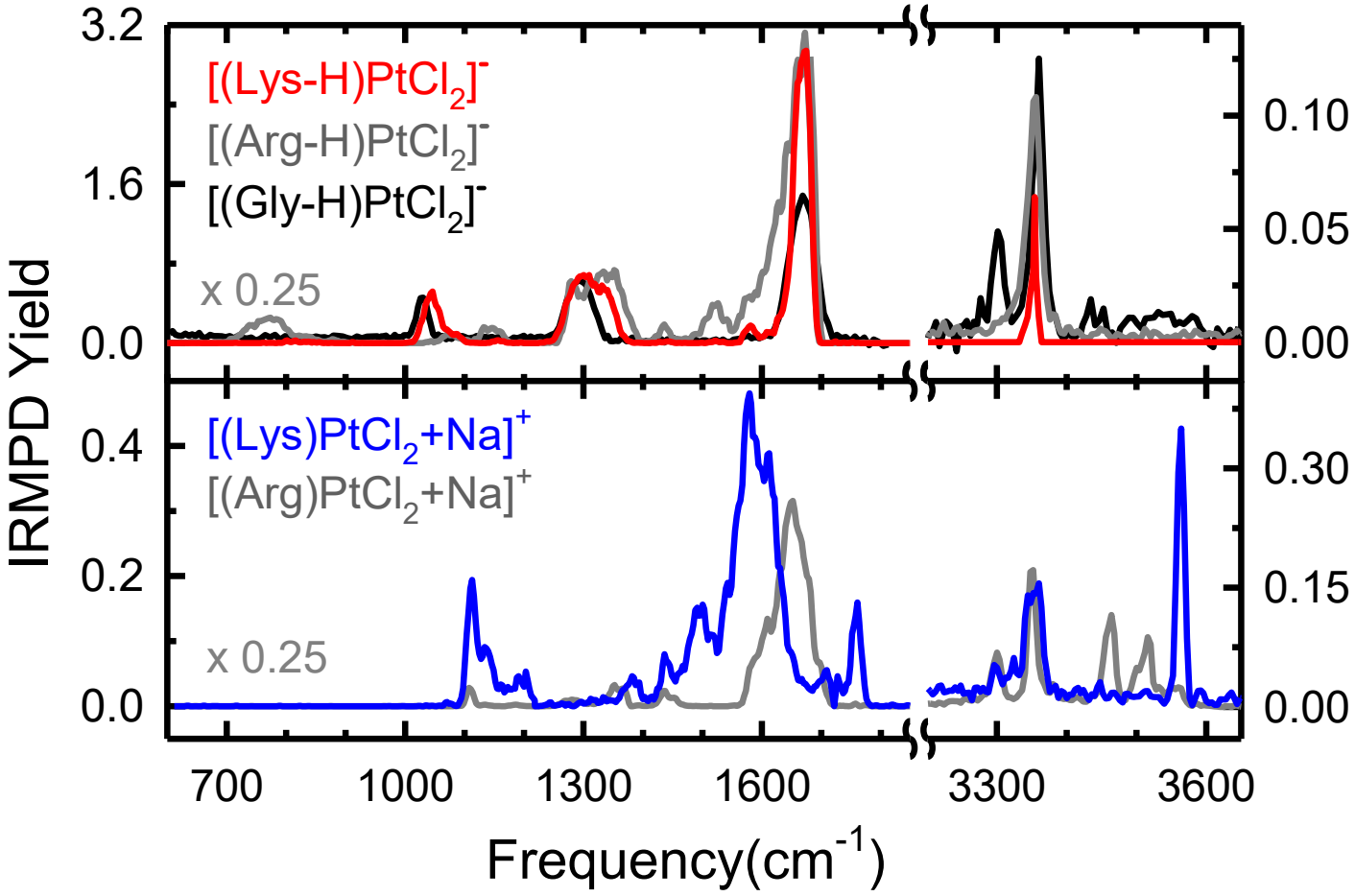
3.2
1.6
0.0
[(Lys-H)PtCl2]-
[(Arg-H)PtCl2]-
[(Gly-H)PtCl2]-
x 0.25
0.10
0.05
0.00
0.4
0.2
0.0
[(Lys)PtCl2+Na]+
[(Arg)PtCl2+Na]+
x 0.25
0.30
0.15
0.00
IRMPD Yield
700
1000
1300
1600
3300
3600
Frequency(cm-1)

Figure 3.

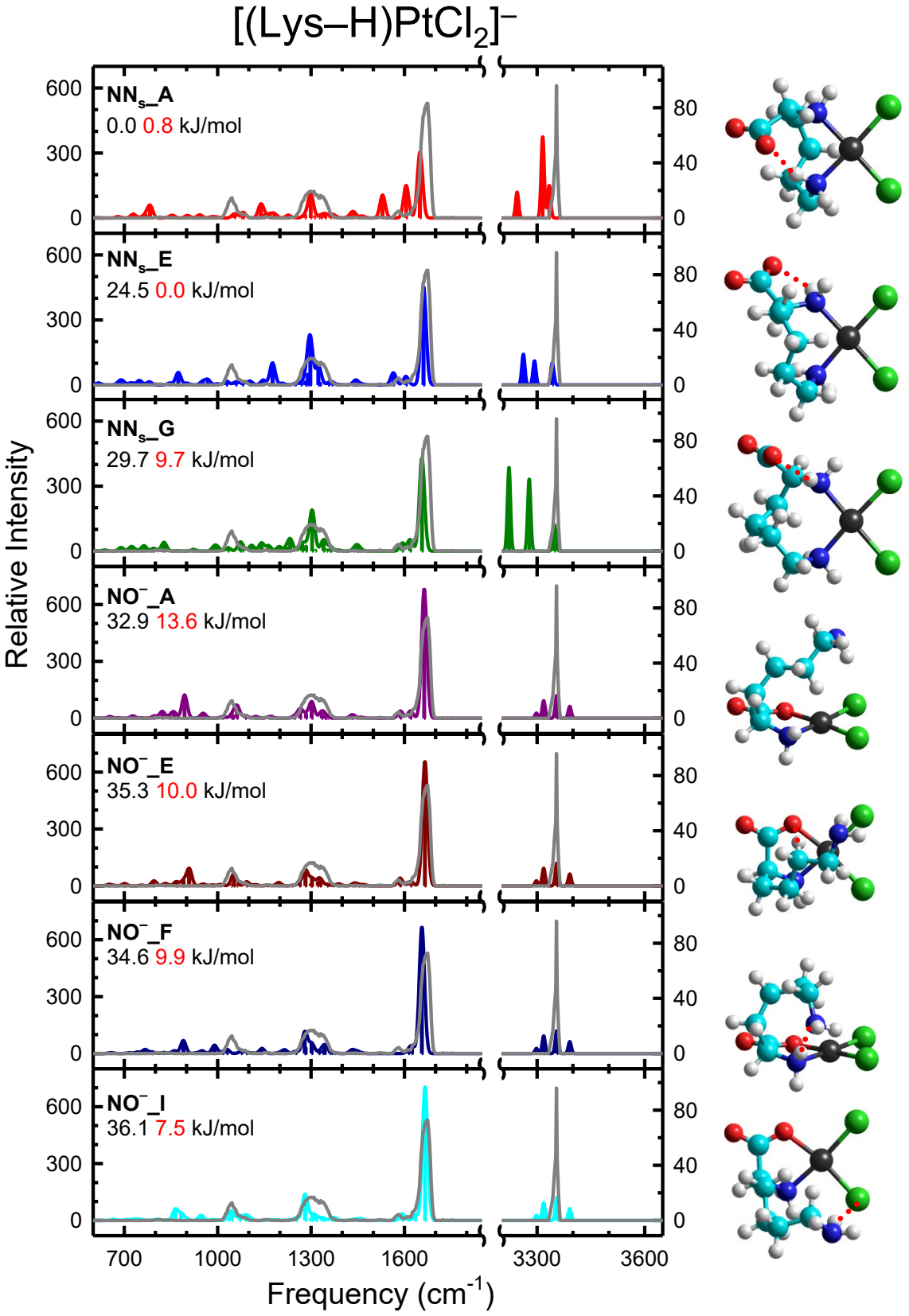
[(Lys–H)PtCl2]–
NNs_A
0.0 0.8 kJ/mol
NNs_E
24.5 0.0 kJ/mol
NNs_G
29.7 9.7 kJ/mol
NO–_A
32.9 13.6 kJ/mol
NO–_E
35.3 10.0 kJ/mol
NO–_F
34.6 9.9 kJ/mol
NO–_I
36.1 7.5 kJ/mol
Relative Intensity
Frequency (cm-1)
700
1000
1300
1600
3300
3600
600
300
0
80
40

Figure 4.

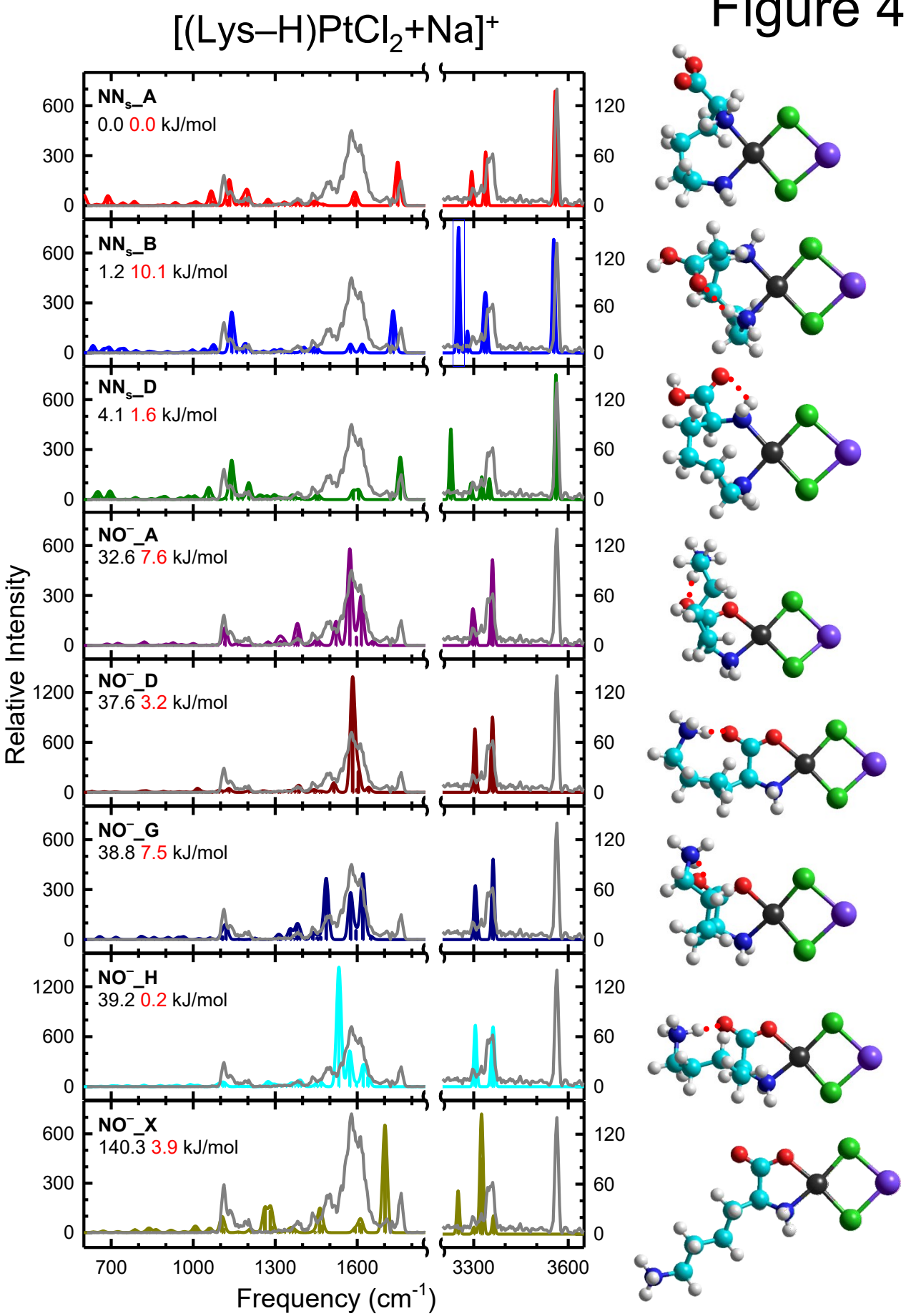
[(Lys–H)PtCl2+Na]+
NNs_A
0.0 0.0 kJ/mol
NNs_B
1.2 10.1 kJ/mol
NNs_D
4.1 1.6 kJ/mol
NO−_A
32.6 7.6 kJ/mol
NO−_D
37.6 3.2 kJ/mol
NO−_G
38.8 7.5 kJ/mol
NO−_H
39.2 0.2 kJ/mol
NO−_X
140.3 3.9 kJ/mol
Relative Intensity
Frequency (cm-1)
700
1000
1300
1600
3300
3600

Scheme 1

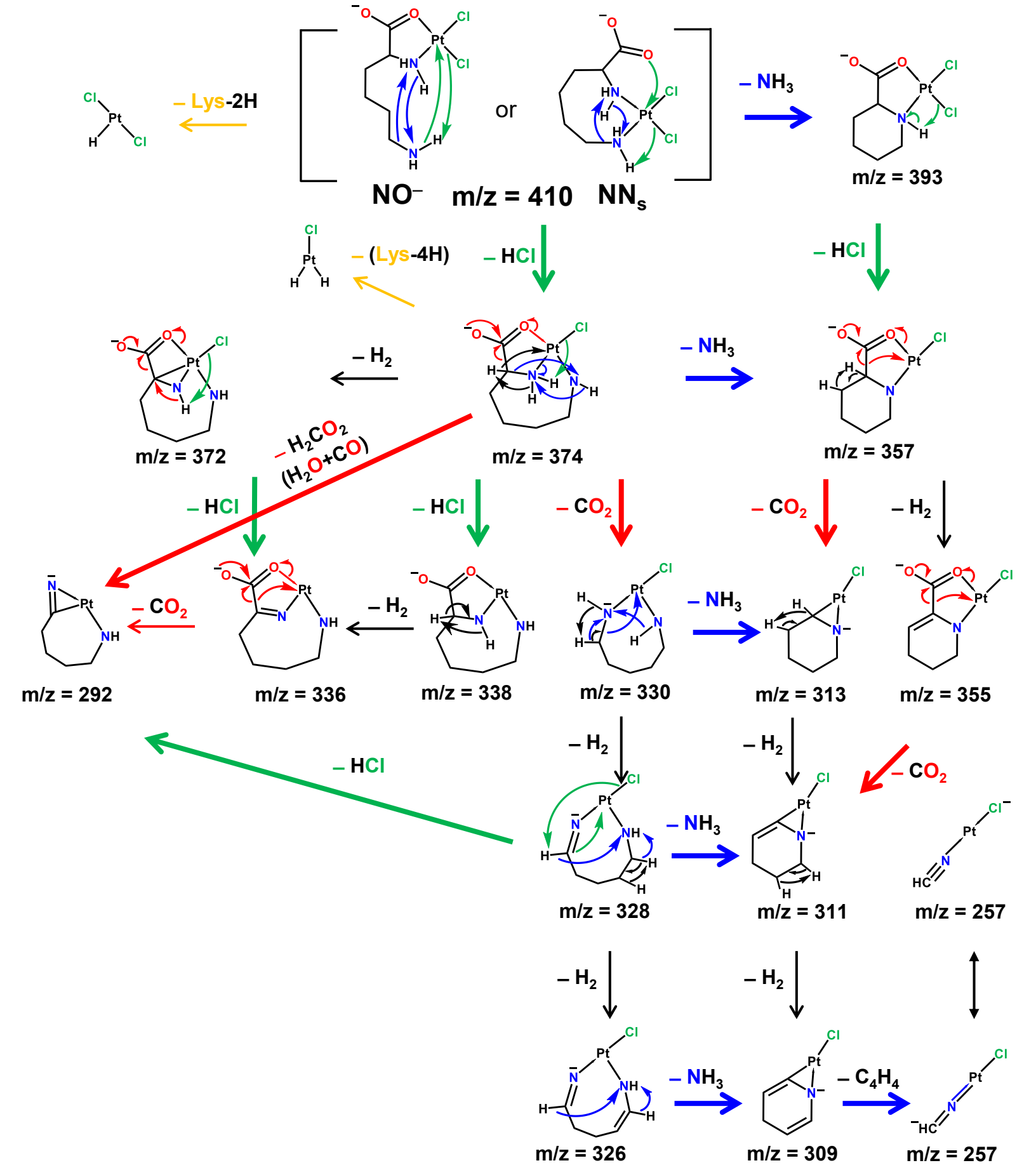
– Lys-2H
or
NO⁻ m/z = 410 NNs
– NH3
m/z = 393
– (Lys-4H)
– HCl
– HCl
– H2
– NH3
m/z = 372
– H2CO2 (H2O+CO)
m/z = 374
m/z = 357
– HCl
– HCl
– CO2
– CO2
– H2
– CO2
– H2
– NH3
– H2
m/z = 292
m/z = 336
m/z = 338
m/z = 330
m/z = 313
m/z = 355
– HCl
– H2
– H2
– CO2
– NH3
m/z = 328
m/z = 311
m/z = 257
– H2
– H2
– NH3
– C4H4
m/z = 326
m/z = 309
m/z = 257

Scheme 2

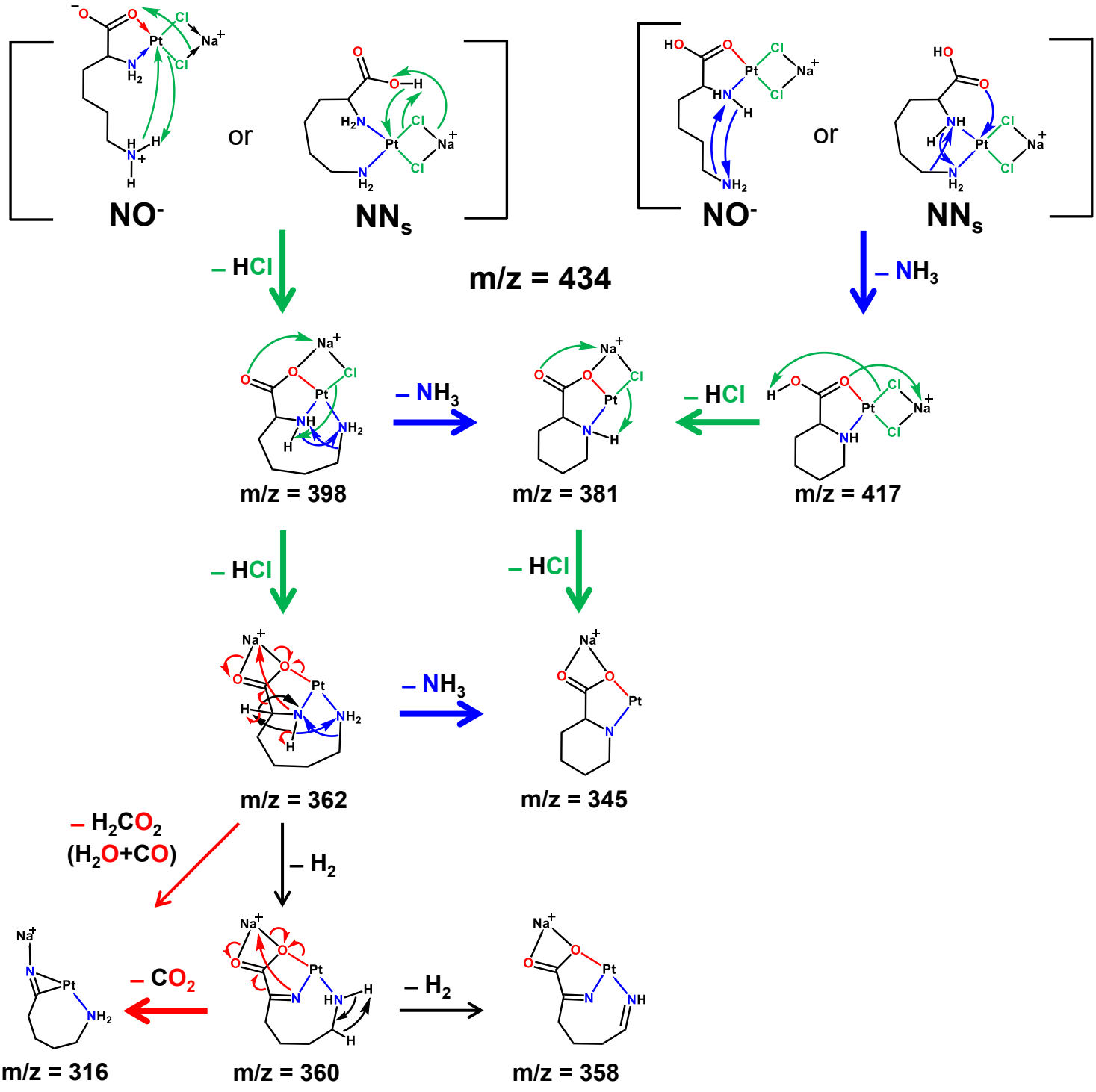
NO-
or
NNs
NO-
or
NNs
– HCl
m/z = 434
– NH3
– NH3
– HCl
m/z = 398
m/z = 381
m/z = 417
– HCl
– HCl
– NH3
m/z = 362
m/z = 345
– H2CO2
(H2O+CO)
– H2
– CO2
– H2
m/z = 316
m/z = 360
m/z = 358

TOC graphic

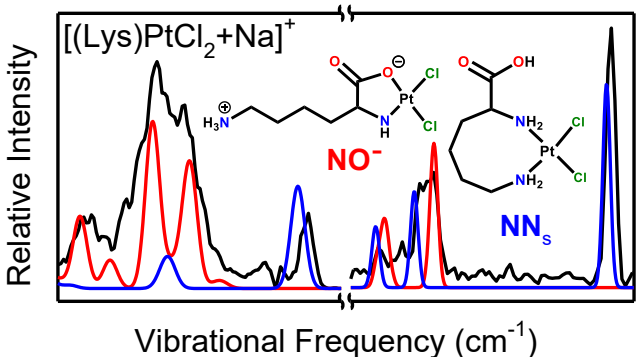
[(Lys)PtCl2+Na]+
NO-
NNS
Relative Intensity
Vibrational Frequency (cm-1)